1 **Title:** Bacterial outer membrane homeostasis via retrograde phospholipid transport

2

3 **Authors:** Rahul Shrivastava[1], Xiang'Er Jiang[1], Shu-Sin Chng[1,2*]

4

5 **Affiliations:**

6 [1]Department of Chemistry, National University of Singapore, Singapore 117543.

7 [2]Singapore Center for Environmental Life Sciences Engineering, National University of

8 Singapore (SCELSE-NUS), Singapore 117456.

9

10 *To whom correspondence should be addressed. E-mail: chmchngs@nus.edu.sg

Abstract:

The outer membrane (OM) is essential for viability in Gram-negative bacteria, yet mechanisms to ensure its stability and homeostasis are not known. The trans-envelope Tol-Pal complex, whose physiological role has remained elusive, is important for OM stability, and coordinated OM invagination during cell division. Here, we establish the function of the Tol-Pal complex in OM lipid homeostasis in *Escherichia coli*. Cells lacking the complex exhibit defects in lipid asymmetry and accumulate excess phospholipids (PLs) in the OM. This imbalance in OM lipids is due to defective retrograde PL transport in the absence of a functional Tol-Pal complex. Thus, cells ensure the assembly of a stable OM by maintaining an excess flux of PLs to the OM only to return the surplus to the inner membrane via transport mediated by the Tol-Pal complex. Our findings also provide insights into the mechanism by which the Tol-Pal complex promotes OM invagination during division.

23 **Main Text:**

24 Lipid bilayers define cellular compartments, and thus life itself, yet our understanding
25 of the assembly and maintenance of these structures are limited. In Gram-negative bacteria,
26 the outer membrane (OM) is essential for growth, and allows the formation of an oxidizing
27 periplasmic compartment beyond the cytoplasmic or inner membrane (IM)[1]. The OM is
28 asymmetric, with lipopolysaccharides (LPS) and phospholipids (PLs) found in the outer and
29 inner leaflets, respectively. This unique lipid asymmetry is required for the OM to function as
30 an effective and selective permeability barrier against toxic substances, rendering Gram-
31 negative bacteria intrinsically resistant to many antibiotics, and allowing survival under
32 adverse conditions. The assembly pathways of various OM components, including LPS[2], β-
33 barrel OM proteins (OMPs)[3], and lipoproteins[4], have been well-characterized; however,
34 processes by which PLs are assembled into the OM have not been discovered. Even though
35 they are the most basic building blocks of any lipid bilayer, essentially nothing is known
36 about how PLs are transported between the IM and the OM. Unlike other OM components,
37 PL movement between the two membranes is bidirectional[5, 6, 7]. While anterograde (IM-to-
38 OM) transport is essential for OM biogenesis, the role for retrograde (OM-to-IM) PL
39 transport is unclear. How assembly of the various OM components are coordinated to ensure
40 homeostasis and stability of the OM is also unknown.

41 The Tol-Pal complex is a trans-envelope system highly conserved in Gram-negative
42 bacteria[8, 9]. It comprises five proteins organized in two sub-complexes, TolQRA in the IM
43 and TolB-Pal at the OM. In *Escherichia coli*, these sub-complexes interact in a proton motive
44 force (pmf)-dependent fashion, with TolQR transducing energy to control conformational
45 changes in TolA and allowing it to reach across the periplasm to contact Pal[10, 11], an OM
46 lipoprotein that binds peptidoglycan[12]. TolA also interacts with periplasmic TolB[13], whose
47 function within the complex is not clear. The TolQRA sub-complex is analogous to the

48 ExbBD-TonB system[8, 14, 15], where energy-dependent conformational changes in TonB are
49 exploited for the transport of metal-siderophores across the OM[16]. Unlike the ExbBD-TonB
50 system, however, the physiological role of the Tol-Pal complex has not been elucidated,
51 despite being discovered over four decades ago[17, 18]. The Tol-Pal complex has been shown to
52 be important for OM invagination during cell division[19], but mutations in the *tol-pal* genes
53 also result in a variety of phenotypes, such as hypersensitivity to detergents and antibiotics,
54 leakage of periplasmic proteins, and prolific shedding of OM vesicles, all indicative of an
55 unstable OM[8]. In addition, removing the *tol-pal* genes causes envelope stress and up-
56 regulation of the σ^E and Rcs phosphorelay responses[20, 21]. It has thus been suggested that the
57 Tol-Pal complex may in fact be important for OM stability and biogenesis. Interestingly, the
58 *tol-pal* genes are often found in the same operon as *ybgC*[9], which encodes an acyl
59 thioesterase shown to interact with PL biosynthetic enzymes in *E. coli*[22]. This association
60 suggests that the Tol-Pal complex may play a role in PL metabolism and/or transport.
61

62 **Cells lacking the Tol-Pal complex exhibit defects in OM lipid asymmetry**

63 To elucidate the function of the Tol-Pal complex, we set out to characterize the
64 molecular nature of OM defects observed in *tol-pal* mutants in *E. coli*. Defects in the
65 assembly of OM components typically lead to perturbations in OM lipid asymmetry[23, 24]. This
66 is characterized by the accumulation of PLs in the outer leaflet of the OM, which serve as
67 substrates for PagP-mediated acylation of LPS (lipid A)[25]. To determine if *tol-pal* mutants
68 exhibit defects in OM lipid asymmetry, we analyzed lipid A acylation in strains lacking any
69 member of the Tol-Pal complex. We demonstrated that each of the mutants accumulate more
70 hepta-acylated lipid A in the OM compared to wild-type (WT) cells (Fig. 1). This OM defect,
71 and the resulting SDS/EDTA sensitivity in these *tol-pal* mutants, are all corrected in the
72 complemented strains (Fig. 1, Extended Data Fig. 1). We also examined other strains with

73 known OM permeability defects. We detected increased lipid A acylation in strains with
74 either impaired OMP (*bamB*, *bamD*, Δ*surA*) or LPS (*lptD4213*) biogenesis, as would be
75 expected, but not in strains lacking covalent tethering between the cell wall and the OM
76 (Δ*lpp*) (Fig. 1). Even though the Δ*lpp* mutant is known to exhibit pleiotropic phenotypes
77 similar to the *tol-pal* mutants[26, 27], it does not have perturbations in OM lipid asymmetry. In
78 contrast to OMP or LPS assembly mutants, *tol-pal* strains produce WT levels of major OMPs
79 and LPS in the OM (Extended Data Fig. 2). These results indicate that *tol-pal* mutations lead
80 to accumulation of PLs in the outer leaflet of the OM independent of OMP and LPS
81 biogenesis pathways.
82

83 **Cells lacking the Tol-Pal complex have disrupted OM lipid homeostasis**

84 We hypothesized that the loss of OM lipid asymmetry in *tol-pal* mutants is due to
85 defects in PL transport across the cell envelope. To test this, we examined the steady-state
86 distribution of PLs (specifically labelled with [^{3}H]-glycerol) between the IM and the OM in
87 WT and *tol-pal* strains. We established that *tol-pal* mutants have ~1.4-1.6-fold more PLs in
88 their OMs (relative to the IMs) than the WT strain (Fig. 2a, Extended Data Fig. 4). To
89 ascertain if this altered distribution of PLs between the two membranes was due to the
90 accumulation of more PLs in the OMs of *tol-pal* mutants, we quantified the ratios of PLs to
91 LPS (both lipids now labelled with [^{14}C]-acetate) following OM isolation and differential
92 extraction. *tol-pal* mutants contain ~1.5-2.5-fold more PLs (relative to LPS) in their OMs,
93 when compared to the WT strain (Fig. 2b, Extended Data Fig. 5). Since *tol-pal* mutants
94 produce WT LPS levels (Extended Data Fig. 2b), we conclude that strains lacking the Tol-Pal
95 complex accumulate excess PLs in their OMs, a phenotype that can be corrected via genetic
96 complementation (Fig. 2). Consistent with this idea, *tol-pal* mutants, unlike WT[28], are able to
97 survive the toxic effects of LPS overproduction (Extended Data Fig. 6), possibly due to a

more optimal balance of PLs to LPS in their OMs. Importantly, having excess PLs makes the OM unstable, and can account for the permeability and vesiculation phenotypes observed in *tol-pal* mutants[8, 27]. Furthermore, cells lacking the Tol-Pal complex are on average shorter and wider than WT cells (when grown under conditions with no apparent division defects)[19]; this reflects an increase in surface area of the rod-shaped cells, possibly a result of increase in OM lipid content. As expected, we did not observe disruption of lipid homeostasis in the Δ*lpp* mutant (Fig. 2). However, we observed higher PL content in the OMs of strains defective in OMP assembly. We reasoned that this increase may help to stabilize the OM by filling the voids created by the decrease in properly-assembled OMPs. Since strains lacking the Tol-Pal complex have proper OMP assembly (Extended Data Fig. 2a), the phenotype of excess PL build-up in the OM must be due to a different problem. Our results suggest that *tol-pal* mutations directly affect PL transport processes, and therefore OM lipid homeostasis.

Cells lacking the Tol-Pal complex are defective in retrograde PL transport

Unlike for other OM components, PL transport between the IM and the OM is bidirectional[5, 6, 7]. Therefore, a simple explanation for the accumulation of excess PLs in the OMs of cells lacking the Tol-Pal complex is that there are defects in retrograde PL transport. To evaluate this possibility, we used the turnover of OM PLs (specifically anionic lipids, including phosphatidylserine (PS), phosphatidylglycerol (PG), and cardiolipin (CL)) as readout for the transport of PLs back to the IM (Fig. 3a). As an intermediate during the biosynthesis of the major lipid phosphatidylethanolamine (PE), PS is converted to PE by the PS decarboxylase (PSD) at the IM, and typically exists only at trace levels[29]. PG and CL have relatively short lifetimes[30, 31]. While the pathways for CL turnover are not known, PG can be converted to PE via PS[32]. Since all known enzymes involved in possible pathways of converting PG to PS, and then to PE, are localized in the IM[29], the turnover of OM anionic

123 lipids require, and therefore report on, retrograde PL transport. Such an assay has previously
124 been employed to demonstrate retrograde transport for PS[7].

125 Using a strain expressing a temperature-sensitive (Ts) allele (*psd2*) of the gene
126 encoding PSD[33], we pulse-labelled PLs with [^{32}P]-phosphate at the restrictive temperature
127 (42˚C), and monitored the turnover of individual PL species in the OM during a chase period
128 at the permissive temperature (30˚C). At 42˚C, the *psd2* strain accumulates substantial
129 amounts of PS in both the IM and the OM (Fig. 3b, 0-min time point), as previously
130 reported[33]. With the restoration of PSD activity at 30˚C, we observed initial increase but
131 eventual conversion of PS to PE in both membranes (Fig. 3b, after 45-min time point),
132 indicating that OM PS is transported back to the IM, converted to PE, and subsequently re-
133 equilibrated to the OM[7]. We also detected higher PG/CL content in the *psd2* strain at 42˚C,
134 and saw rapid conversion of these lipids to PE in both membranes at 30˚C (Fig. 3b), at rates
135 comparable to what was previously reported (for PG)[32]. The fact that PS levels increase
136 initially but decrease after 45 min into the chase is consistent with the idea that PS is an
137 intermediate along the turnover pathway for PG[32], as well as for CL. To confirm this
138 observation, we also performed the chase at 42˚C in the presence of a known PSD inhibitor[34]
139 (these conditions completely shut down PSD activity), and found quantitative conversion of
140 PG/CL to PS in both membranes (Extended Data Fig. 7). We further showed that PG/CL-to-
141 PE conversion is abolished in the presence of the pmf uncoupler carbonyl cyanide *m*-
142 chlorophenyl hydrazone (CCCP)(Fig. 3c), demonstrating a requirement for cellular energy
143 sources in this process[32], and that conversion occurs in the IM. The observation of PG/CL
144 turnover in the IM is thus expected. The fact that we also observed the conversion of OM
145 PG/CL to PE points towards an intact retrograde PL transport pathway for these lipids in the
146 otherwise WT cells. Notably, turnover of OM PG/CL appears to be slightly faster than that of

147 IM PG/CL (Fig. 3b), suggesting that retrograde transport of these lipids may be coupled to
148 the turnover process.

149 We performed the same pulse-chase experiments with *psd2* cells lacking TolA. We
150 detected PG/CL-to-PE conversion in the IM at rates comparable to WT (Fig. 3d, f; ~67% and
151 ~71% PG/CL turnover at 2 h-chase in Δ*tolA* and WT IMs, respectively (Fig. 4a)),
152 demonstrating that there are functional PG/CL turnover pathways in the Δ*tolA* mutant. In
153 contrast, we observed substantial reduction of the turnover of OM PG/CL in these cells (Fig.
154 3d, f; ~53% PG/CL turnover at 2 h-chase in the Δ*tolA* OM, compared to ~79% for WT (Fig.
155 4a)), even though PS conversion to PE appears intact. These results indicate an apparent
156 defect in the movement of PG and CL (but not PS) from the OM back to the IM, which is
157 restored when complemented with functional $tolA_{WT}$ (Fig. 3e, f, Fig. 4a). Δ*tolR* mutant cells
158 exhibit the same defect, and can similarly be rescued by complementation with functional
159 $tolR_{WT}$ (Fig. 4a). In contrast, no rescue was observed when Δ*tolR* was complemented using a
160 *tolR* allele with impaired ability to utilize the pmf ($tolR_{D23R}$)[14] (Fig. 4a, Extended Data Fig. 1);
161 this indicates that Tol-Pal function is required for efficient PG/CL transport. We also
162 examined PG/CL turnover in *psd2* cells lacking BamB, which accumulate excess PLs in the
163 OM due to defects in OMP assembly (Fig. 2). Neither IM nor OM PG/CL turnover is affected
164 (Fig. 4a), highlighting the different basis for OM PL accumulation in this strain compared to
165 the *tol-pal* mutants. Our assay does not report on the retrograde transport of major lipid PE,
166 which is relatively stable[30]. However, since *tol-pal* mutants accumulate ~1.5-fold more PLs
167 in the OM (Fig. 2) without gross changes in PL composition (compared to WT) (Extended
168 Data Fig. 9), PE transport must also have been affected. We conclude that the Tol-Pal
169 complex is required for the retrograde transport of bulk PLs in *E. coli*.

170 Removing the Tol-Pal complex does not completely abolish retrograde PG/CL
171 transport, indicating that there are other systems involved in this process. The OmpC-Mla

172 system is important for the maintenance of OM lipid asymmetry, and is proposed to do so via
173 retrograde PL transport[35, 36]. We showed that cells lacking MlaC, the periplasmic lipid
174 chaperone in the OmpC-Mla system, do not exhibit defects in OM PG/CL turnover (Fig. 4a).
175 In addition, removing MlaC in cells lacking the Tol-Pal complex does not appear to
176 exacerbate the defects in retrograde PL transport, given that overall turnover rates of IM and
177 OM PG/CL are similarly reduced in the double mutant. These results indicate that the OmpC-
178 Mla system may not contribute significantly to retrograde transport of bulk lipids when
179 expressed at physiological levels, as has been previously suggested[35]. When MlaC and the IM
180 MlaFEDB complex[37] are overexpressed, however, we detected partial rescue of OM PG/CL
181 turnover in the Δ*tolA* mutant (Fig. 4b). Further to validating the putative PL transport
182 function of the OmpC-Mla system, this observation lends strong support to the notion that the
183 Tol-Pal complex is indeed a major system for retrograde PL transport.
184

185 **Discussion**

186 Our work reveals that the Tol-Pal complex plays an important role in maintaining OM
187 lipid homeostasis via retrograde PL transport. Removing the system causes accumulation of
188 excess PLs (over LPS) in the OM (Fig. 2). While pathways for anterograde PL transport
189 remain to be discovered, this result indicates that PL flux to the OM may be intrinsically
190 higher than that of LPS. Evidently, the ability to transport high levels of PLs to the OM
191 allows cells to compensate for the loss of OMPs due to defects in assembly (Fig. 2). Our data
192 suggest that cells maintain an excess flux of PLs to the OM in order to offset changes in the
193 unidirectional assembly pathways for other OM components, and then return the PL surplus
194 to the IM via the Tol-Pal complex (and other redundant systems). Having bidirectional PL
195 transport therefore provides a mechanism to regulate and ensure the formation of a stable
196 OM.

197 It is not clear how the Tol-Pal complex may mediate retrograde PL transport. It is
198 possible that this machine directly binds and transports lipids, although there are no obvious
199 lipid binding motifs or cavities found in available structures of the periplasmic components[38,
200 39]. The Tol-Pal complex is related to the ExbBD-TonB[14, 40], Agl-Glt[41], and Mot[14, 42] systems,
201 each of which uses pmf-energized conformational changes to generate force for the uptake of
202 metal-siderophores, for gliding motility, or to power flagella rotation, respectively. In
203 addition, both the Tol-Pal and ExbBD-TonB complexes are hijacked by toxins (such as
204 colicins) and bacteriophages to penetrate the OM[43]. It is therefore also possible that the Tol-
205 Pal complex acts simply as a force generator to transport other PL-binding proteins across the
206 periplasm, or perhaps bring the OM close enough to the IM for PL transfer to occur via
207 hemifusion events. For the latter scenario, one can envision energized TolA pulling the OM
208 inwards via its interaction with Pal, which is anchored to the inner leaflet of the OM[12]. While
209 it remains controversial, the formation of such "zones of adhesion", or membrane contact
210 sites, has previously been proposed[44], and in fact, was suggested to be a mechanism for
211 retrograde transport of native and foreign lipids[6].

212 That the Tol-Pal complex is involved in retrograde PL transport also has significant
213 implications for Gram-negative bacterial cell division. As part of the divisome, this system is
214 important for proper OM invagination during septum constriction[19, 45, 46]. How OM
215 invagination occurs is unclear. Apart from physically tethering the IM and the OM, we
216 propose that removal of PLs from the inner leaflet of the OM by the Tol-Pal complex serves
217 to locally reduce the surface area of the inner leaflet relative to the outer leaflet[47]. According
218 to the bilayer-couple model[48], this may then induce the requisite negative curvature in the
219 OM at the constriction site, thus promoting formation of the new cell poles.

220 Given the importance of the Tol-Pal complex in OM stability and bacterial cell
221 division, it would be an attractive target for small molecule inhibition. This is especially so in

222 some organisms, including the opportunistic human pathogen *Pseudomonas aeruginosa*,
223 where the complex is essential for growth[49, 50]. The lack of understanding of the true role of
224 the Tol-Pal complex, however, has impeded progress. We believe that our work in
225 elucidating the physiological function of this complex will accelerate efforts in this direction,
226 and contribute towards the development of new antibiotics in our ongoing fight against
227 recalcitrant Gram-negative infections.
228

229 **References**

230 1. Nikaido, H. Molecular basis of bacterial outer membrane permeability revisited.
231 *Microbiol. Mol. Biol. Rev.* **67**, 593-656 (2003)
232 2. Okuda, S., Sherman, D. J., Silhavy, T. J., Ruiz, N. & Kahne, D. Lipopolysaccharide
233 transport and assembly at the outer membrane: the PEZ model. *Nat. Rev. Microbiol.*
234 **14**, 337-345 (2016)
235 3. Hagan, C. L., Silhavy, T. J. & Kahne, D. β-barrel membrane protein assembly by the
236 Bam complex. *Annu. Rev. Biochem.* **80**, 189-210 (2011)
237 4. Okuda, S. & Tokuda, H. Lipoprotein sorting in bacteria. *Annu. Rev. Microbiol.* **65**,
238 239-259 (2011)
239 5. Donohue-Rolfe, A. M. & Schaechter, M. Translocation of phospholipids from the
240 inner to the outer membrane of *Escherichia coli*. *Proc. Natl. Acad. Sci. U.S.A.* **77**,
241 1867-1871 (1980)
242 6. Jones, N. C. & Osborn, M. J. Translocation of phospholipids between the outer and
243 inner membranes of *Salmonella typhimurium*. *J. Biol. Chem.* **252**, 7405-7412 (1977)
244 7. Langley, K. E., Hawrot, E. & Kennedy, E. P. Membrane assembly: movement of
245 phosphatidylserine between the cytoplasmic and outer membranes of *Escherichia*
246 *coli*. *J. Bacteriol.* **152**, 1033-1041 (1982)

247 8. Lloubes, R. *et al.* The Tol-Pal proteins of the *Escherichia coli* cell envelope: an
248 energized system required for outer membrane integrity? *Res. Microbiol.* **152**, 523-
249 529 (2001)
250 9. Sturgis, J. N. Organisation and evolution of the *tol-pal* gene cluster. *J. Mol.*
251 *Microbiol. Biotechnol.* **3**, 113-122 (2001)
252 10. Cascales, E., Gavioli, M., Sturgis, J. N. & Lloubes, R. Proton motive force drives the
253 interaction of the inner membrane TolA and outer membrane Pal proteins in
254 *Escherichia coli*. *Mol. Microbiol.* **38**, 904-915 (2000)
255 11. Germon, P., Ray, M. C., Vianney, A. & Lazzaroni, J. C. Energy-dependent
256 conformational changes in the TolA protein of *Escherichia coli* involves its N-
257 terminal domain, TolQ, and TolR. *J. Bacteriol.* **183**, 4110-4114 (2001)
258 12. Godlewska, R., Wisniewska, K., Pietras, Z. & Jagusztyn-Krynicka, E. K.
259 Peptidoglycan-associated lipoprotein (Pal) of Gram-negative bacteria: function,
260 structure, role in pathogenesis and potential application in immunoprophylaxis. *FEMS*
261 *Microbiol. Lett.* **298**, 1-11 (2009)
262 13. Walburger, A., Lazdunski, C. & Corda, Y. The Tol/Pal system function requires an
263 interaction between the C-terminal domain of TolA and the N-terminal domain of
264 TolB. *Mol. Microbiol.* **44**, 695-708 (2002)
265 14. Cascales, E., Lloubes, R. & Sturgis, J. N. The TolQ-TolR proteins energize TolA and
266 share homologies with the flagellar motor proteins MotA-MotB. *Mol. Microbiol.* **42**,
267 795-807 (2001)
268 15. Witty, M. *et al.* Structure of the periplasmic domain of *Pseudomonas aeruginosa*
269 TolA: evidence for an evolutionary relationship with the TonB transporter protein.
270 *EMBO J.* **21**, 4207-4218 (2002)

271 16. Gresock, M. G., Kastead, K. A. & Postle, K. From homodimer to heterodimer and
272 back: elucidating the TonB energy transduction cycle. *J. Bacteriol.* **197**, 3433-3445
273 (2015)
274 17. Bernstein, A., Rolfe, B. & Onodera, K. Pleiotropic properties and genetic organization
275 of the *tolA, B* locus of *Escherichia coli* K-12. *J. Bacteriol.* **112**, 74-83 (1972)
276 18. Lazzaroni, J. C. & Portalier, R. C. Genetic and biochemical characterization of
277 periplasmic-leaky mutants of *Escherichia coli* K-12. *J. Bacteriol.* **145**, 1351-1358
278 (1981)
279 19. Gerding, M. A., Ogata, Y., Pecora, N. D., Niki, H. & de Boer, P. A. J. The trans-
280 envelope Tol-Pal complex is part of the cell division machinery and required for
281 proper outer-membrane invagination during cell constriction in *E. coli*. *Mol.*
282 *Microbiol.* **63**, 1008-1025 (2007)
283 20. Vines, E. D., Marolda, C. L., Balachandran, A. & Valvano, M. A. Defective O-
284 antigen polymerization in *tolA* and *pal* mutants of *Escherichia coli* in response to
285 extracytoplasmic stress. *J. Bacteriol.* **187**, 3359-3368 (2005)
286 21. Clavel, T., Lazzaroni, J. C., Vianney, A. & Portalier, R. Expression of the *tolQRA*
287 genes of *Escherichia coli* K-12 is controlled by the RcsC sensor protein involved in
288 capsule synthesis. *Mol. Microbiol.* **19**, 19-25 (1996)
289 22. Gully, D. & Bouveret, E. A protein network for phospholipid synthesis uncovered by
290 a variant of the tandem affinity purification method in *Escherichia coli*. *Proteomics* **6**,
291 282-293 (2006)
292 23. Wu, T. *et al*. Identification of a protein complex that assembles lipopolysaccharide in
293 the outer membrane of *Escherichia coli*. *Proc. Natl. Acad. Sci. U.S.A.* **103**, 11754-
294 11759 (2006)

295 24. Ruiz, N., Gronenberg, L. S., Kahne, D. & Silhavy, T. J. Identification of two inner-
296 membrane proteins required for the transport of lipopolysaccharide to the outer
297 membrane of *Escherichia coli*. *Proc. Natl. Acad. Sci. U.S.A.* **105**, 5537-5542 (2008)
298 25. Bishop, R. E. The lipid A palmitoyltransferase PagP: molecular mechanisms and role
299 in bacterial pathogenesis. *Mol. Microbiol.* **57**, 900-912 (2005)
300 26. Yem, D. W. & Wu, H. C. Phenotypic characterization of an *Escherichia coli* mutant
301 altered in the structure of murein lipoprotein. *J. Bacteriol.* **133**, 1419-1426 (1978)
302 27. Bernadac, A., Gavioli, M., Lazzaroni, J. C., Raina, S. & Lloubes, R. *Escherichia coli*
303 *tol-pal* mutants form outer membrane vesicles. *J. Bacteriol.* **180**, 4872-4878 (1998)
304 28. Fuhrer, F., Langklotz, S. & Narberhaus, F. The C-terminal end of LpxC is required
305 for degradation by the FtsH protease. *Mol. Microbiol.* **59**, 1025-1036 (2006)
306 29. Cronan, J. E. Bacterial membrane lipids: where do we stand? *Annu. Rev. Microbiol.*
307 **57**, 203-224 (2003)
308 30. Kanfer, J. & Kennedy, E. P. Metabolism and function of bacterial lipids. I.
309 Metabolism of phospholipids in *Escherichia coli* B. *J. Biol. Chem.* **238**, 2919-2922
310 (1963)
311 31. Kanemasa, Y., Akamatsu, Y. & Nojima, S. Composition and turnover of the
312 phospholipids in *Escherichia coli*. *Biochim. Biophys. Acta.* **144**, 382-390 (1967)
313 32. Yokoto, K. & Kito, M. Transfer of the phosphatidyl moiety of phosphatidylglycerol to
314 phosphatidylethanolamine in *Escherichia coli*. *J. Bacteriol.* **151**, 952-961 (1982)
315 33. Hawrot, E. & Kennedy, E. P. Phospholipid composition and membrane function in
316 phosphatidylserine decarboxylase mutants of *Escherichia coli*. *J. Biol. Chem.* **253**,
317 8213-8220 (1978)

318 34. Satre, M. & Kennedy, E. P. Identification of bound pyruvate essential for the activity
319 of phosphatidylserine decarboxylase of *Escherichia coli*. *J. Biol. Chem.* **253**, 479-483
320 (1978)
321 35. Malinverni, J. C. & Silhavy, T. J. An ABC transport system that maintains lipid
322 asymmetry in the Gram-negative outer membrane. *Proc. Natl. Acad. Sci. U.S.A.* **106**,
323 8009-8014 (2009)
324 36. Chong, Z. S., Woo, W. F. & Chng, S. S. Osmoporin OmpC forms a complex with
325 MlaA to maintain outer membrane lipid asymmetry in *Escherichia coli*. *Mol.*
326 *Microbiol.* **98**, 1133-1146 (2015)
327 37. Thong, S. *et al.* Defining key roles for auxillary proteins in an ABC transporter that
328 maintains bacterial outer membrane lipid asymmetry. *eLife* **5**, e19042 (2016)
329 38. Deprez, C. *et al.* Solution structure of the *E. coli* TolA C-termical domain reveals
330 conformational changes upon binding to the phage g3p N-terminal domain. *J. Mol.*
331 *Biol.* **346**, 1047-1057 (2005)
332 39. Carr, S., Penfold, C. N., Bamford, V., James, R. & Hemmings, A. M. The structure of
333 TolB, an essential component of the *tol*-dependent translocation system, and its
334 protein-protein interaction with the translocation domain of colicin E9. *Structure* **8**,
335 57-66 (2000)
336 40. Celia, H. *et al*. Structural insight into the role of the Ton complex in energy
337 transduction. *Nature* **538**, 60-65 (2016)
338 41. Faure, L. M. *et al*. The mechanism of force transmission at bacterial focal adhesion
339 complexes. *Nature* **539**, 530-535 (2016)
340 42. Thormann, K. M. & Paulick, A. Tuning the flagellar motor. *Microbiology* **156**, 1275-
341 1283 (2010)
342 43. Cascales, E. *et al.* Colicin biology. *Microbiol. Mol. Biol. Rev.* **71**, 158-229 (2007)

343 44. Bayer, M. E. Zones of membrane adhesion in the cryofixed envelope of *Escherichia*
344 *coli*. *J. Struct. Biol.* **107**, 268-280 (1991)
345 45. Yeh, Y. C., Comolli, L. R., Downing, K. H., Shapiro, L. & McAdams, H. H. The
346 *Caulobacter* Tol-Pal complex is essential for outer membrane integrity and the
347 positioning of a polar localization factor. *J. Bacteriol.* **192**, 4847-4858 (2010)
348 46. Jacquier, N., Frandi, A., Viollier, P. H. & Greub, G. Disassembly of a medial
349 transenvelope structure by antibiotics during intracellular division. *Chem. Bio.* **22**,
350 1217-1227 (2015)
351 47. McMahon, H. T. & Gallop, J. L. Membrane curvature and mechanisms of dynamic
352 cell membrane remodelling. *Nature* **438**, 590-596 (2005)
353 48. Sheetz, M. P. & Singer, S. J. Biological membranes as bilayer couples. A molecular
354 mechanism of drug-erythrocyte interactions. *Proc. Natl. Acad. Sci. U.S.A.* **71**, 4457-
355 4461 (1974)
356 49. Dennis, J. J., Lafontaine, E. R. & Sokol, P. A. Identification and characterization of
357 the *tolQRA* genes of *Pseudomonas aeruginosa*. *J. Bacteriol.* **178**, 7059-7068 (1996)
358 50. Lo Sciuto, A. *et al.* The periplasmic protein TolB as a potential drug target in
359 *Pseudomonas aeruginosa*. *PLoS One* **9**, e103784 (2014)

360 **Acknowledgments.** We thank Zhi-Soon Chong for constructing the Δ*mlaC* allele, and
361 Manjula Reddy (Center for Cellular and Molecular Biology) for providing the *lpxC1272*
362 mutant and the p*yciM* plasmid. We thank Chee-Geng Chia for performing preliminary
363 experiments. We are grateful to Swaine Chen (NUS), Rajeev Misra (Arizona State U), and
364 Daniel Kahne (Harvard U) for their generous gifts of α-OmpC, α-OmpF, and α-LptE and α-
365 BamA antibodies, respectively. Finally, we thank William F. Burkholder (Institute of
366 Molecular and Cell Biology) and Jean-Francois Collet (U catholique de Louvain) for critical
367 comments and suggestions on the manuscript. This work was supported by the National
368 University of Singapore Start-up funding, the Singapore Ministry of Education Academic
369 Research Fund Tier 1 grant, and the Singapore Ministry of Health National Medical Research
370 Council under its Cooperative Basic Research Grant (NMRC/CBRG/0072/2014) (to S.-S.C.).
371

372 **Author contributions.** R.S. performed all experiments described in this work; X.E.J.
373 performed experiments related to LpxC overexpression; R.S. and S.-S.C. analyzed and
374 discussed data; R.S. and S.-S.C. wrote the paper.
375

376 **Competing financial interests.** The authors declare no conflict of interest.

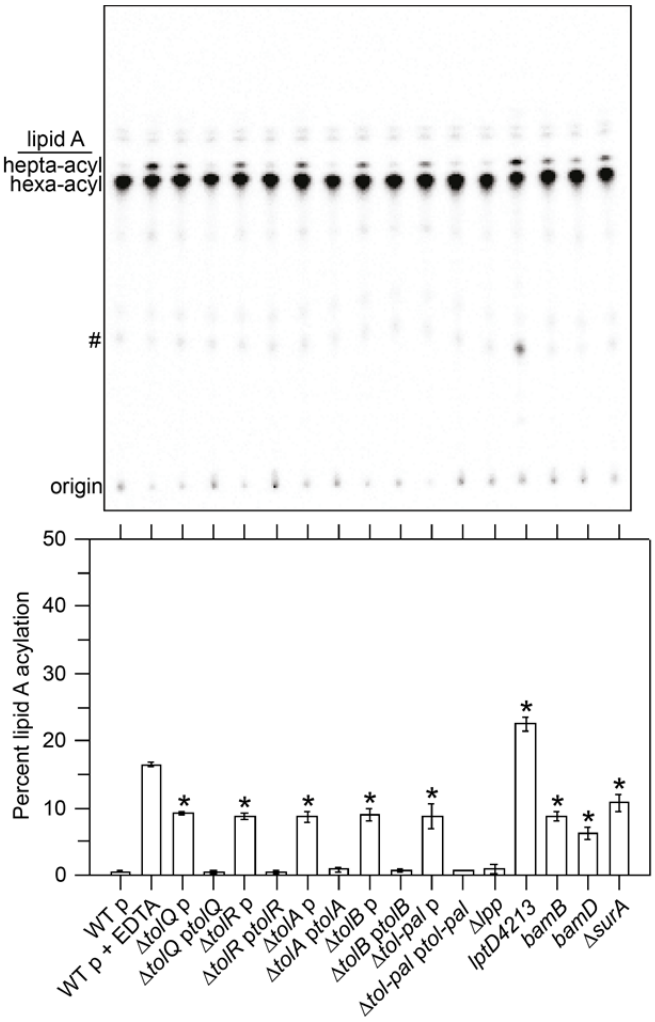

Figure 1 | Cells lacking the Tol-Pal complex accumulate PLs in the outer leaflet of the OM, as judged by lipid A acylation. Thin layer chromatographic (TLC) analysis of [^{32}P]-labelled lipid A extracted from WT, Δ*tol-pal*, and various mutant strains (*see text*). Where indicated, WT and *tol-pal* mutants contain an empty pET23/42 plasmid (p)[23] or one expressing the corresponding *tol-pal* gene(s) at low levels (e.g. p*tol-pal*). As a positive control for lipid A acylation, WT cells were treated with EDTA (to chelate Mg^{2+} and destabilize the LPS layer) prior to extraction. Equal amounts of radioactivity were spotted for each sample. Lipid spots annotated # represent 1-pyrophosphoryl-lipid A. Average percentages of lipid A acylation and standard deviations were quantified from triplicate experiments and plotted below. Student's t-tests: * $p < 0.005$ as compared to WT.

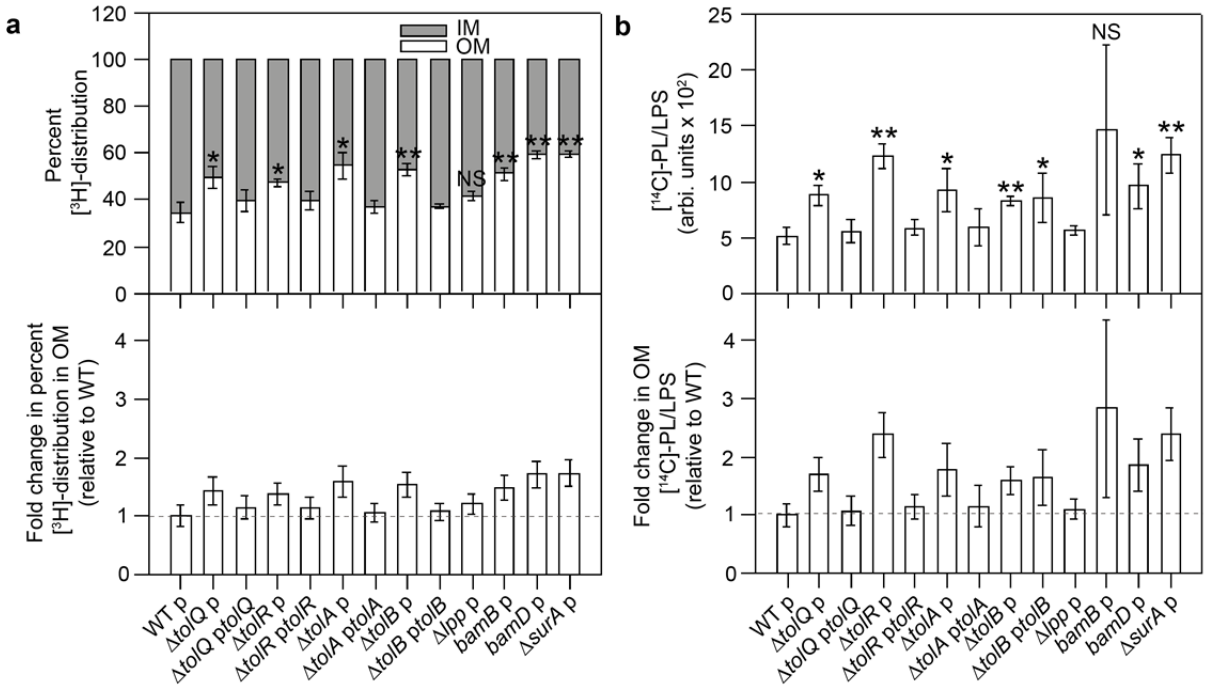

Figure 2 | Cells lacking the Tol-Pal complex accumulate excess PLs (relative to LPS) in the OM. a, Steady-state distribution of [^{3}H]-glycerol labelled PLs between the IM and the OM of WT, Δ*tol-pal*, and various mutant strains (*upper panel*). Distribution of [^{3}H]-labelled PLs in the OMs of respective mutants expressed as fold changes relative to the WT OM (*lower panel*). The IMs and OMs from both WT and *tol-pal* mutants were separated with equal efficiencies during sucrose density gradient fractionation (Extended Data Fig. 3). **b**, Steady-state PL:LPS ratios in the OMs of WT, Δ*tol-pal*, and various mutant strains (*upper panel*). Lipids were labelled with [^{14}C]-acetate and differentially extracted from OMs (Extended Data Fig. 5). OM PL:LPS ratios of respective mutants expressed as fold changes relative to that in the WT OM (*lower panel*). Error bars represent standard deviations calculated from triplicate experiments. Student's t-tests: * $p < 0.05$; ** $p < 0.005$; NS, not significant (as compared to WT).

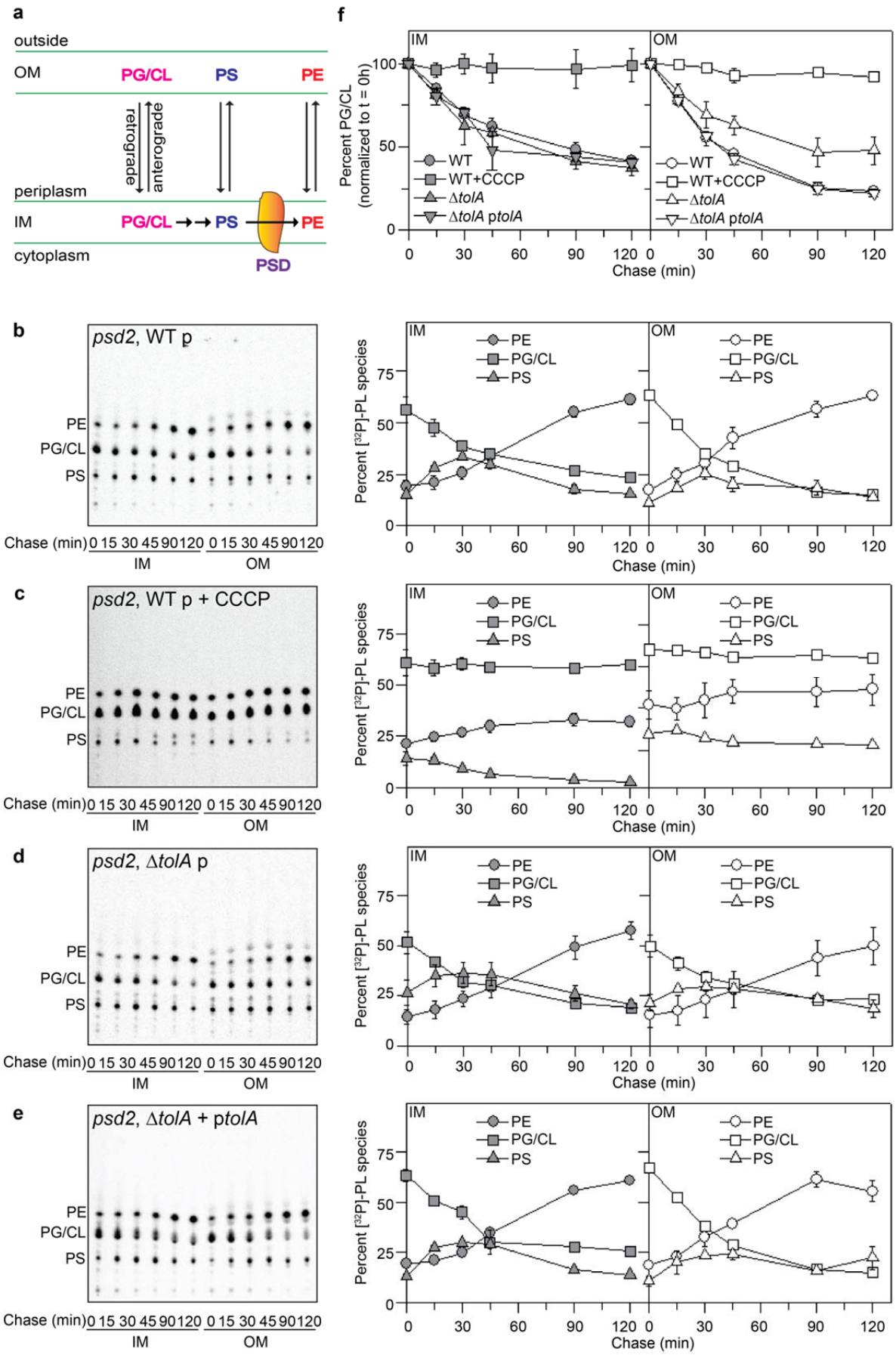
a
outside
OM
PG/CL
PS
PE
retrograde
anterograde
periplasm
IM
PG/CL
PS
PE
cytoplasm
PSD
f
IM
OM
Percent PG/CL (normalized to t = 0h)
WT
WT+CCCP
ΔtolA
ΔtolA ptolA
Chase (min)
b
psd2, WT p
PE
PG/CL
PS
Chase (min) 0 15 30 45 90 120 0 15 30 45 90 120
IM
OM
Percent [32P]-PL species
c
psd2, WT p + CCCP
d
psd2, ΔtolA p
e
psd2, ΔtolA + ptolA

401

402 **Figure 3 | Cells lacking the Tol-Pal complex are defective in OM PG/CL turnover. a**, A
403 schematic diagram depicting movement and turnover of PE, PG and CL (major), and PS
404 (trace) in the cell envelope. **b-e,** TLC time-course analyses of [^{32}P]-pulse-labelled PLs
405 extracted from the IMs and OMs of (**b**) WT, (**c**) WT (with CCCP added), (**d**) Δ*tolA*, and (**e**)
406 *tolA*-complemented strains also harboring the *psd2* mutation. The average percentage levels
407 of PE, PG/CL, and PS in the IM and OM at each time point, together with standard
408 deviations, were quantified from triplicate experiments and shown on the right. **f,** The
409 percentage levels of PG/CL in the IMs and OMs from (**b**)-(**e**) normalized to the
410 corresponding levels at the start of the chase (0 min).

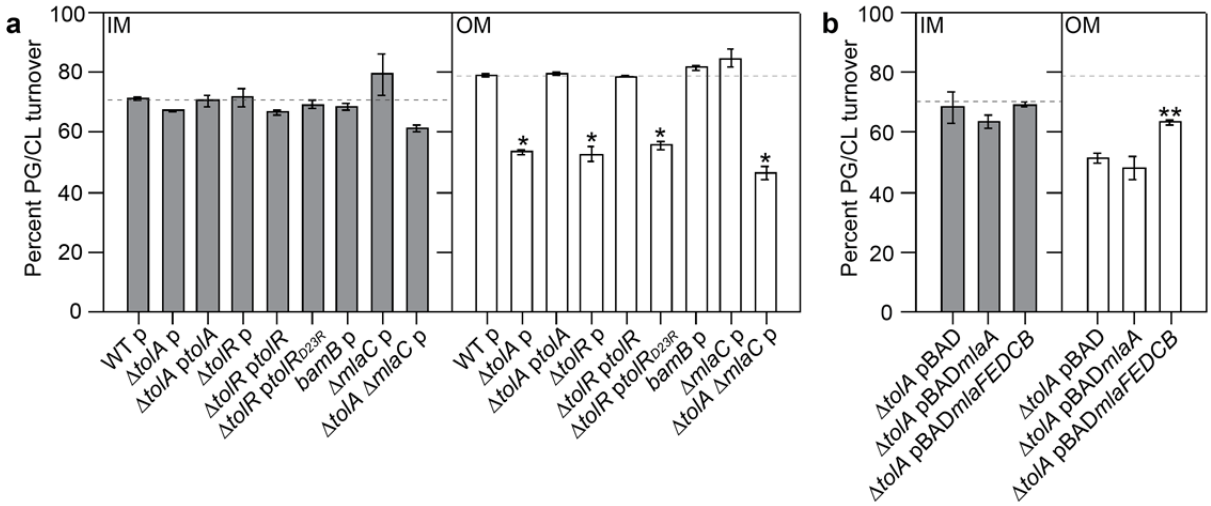

411

412 **Figure 4 | Tol-Pal function is required for efficient retrograde PG/CL transport, as**
413 **judged by OM PG/CL turnover rates.** Single time-point (2-h chase) quantification of the
414 turnover rate of [^{32}P]-labelled PG/CL in the IMs and OMs of (**a**) WT, *tol-pal* and various
415 mutant strains, and (**b**) Δ*tolA* overexpressing OmpC-Mla components, all in the *psd2*
416 background (*see text*) (Extended Data Fig. 8). Percentage PG/CL turnover at 2-h is expressed
417 as $[(\%PG/CL)_{start} - (\%PG/CL)_{2h}]/[(\%PG/CL)_{start}]$. Average percentage lipid levels and
418 standard deviations were quantified from triplicate experiments. Student's t-tests: * $p <$
419 0.0005 as compared to WT; ** $p < 0.0005$ as compared to Δ*tolA*.

420 **Methods**

421

422 **Bacterial strains and growth conditions.** All the strains used in this study are listed in
423 Supplementary Table 1. *Escherichia coli* strain MC4100 [*F⁻ araD139* Δ*(argF-lac) U169*
424 *rpsL150 relA1 flbB5301 ptsF25 deoC1 ptsF25 thi*][51] was used as the wild-type (WT) strain
425 for most of the experiments. To achieve accumulation of phosphatidylserine (PS) in cells, a
426 temperature-sensitive phosphatidylserine decarboxylase mutant (*psd2*), which accumulates
427 PS at the non-permissive temperature, was used[33]. NR754, an *araD*$^+$ revertant of MC4100[24],
428 was used as the WT strain for experiments involving overexpression of *lpxC* from the
429 arabinose-inducible promoter (P_{BAD}). Δ*tolQ*, Δ*tolA* and Δ*tol-pal* deletions were constructed
430 using recombineering[52] and all other gene deletion strains were obtained from the Keio
431 collection[53]. Whenever needed, the antibiotic resistance cassettes were flipped out as
432 described[52]. Gene deletion cassettes were transduced into relevant genetic background strains
433 via P1 transduction[54]. Luria-Bertani (LB) broth (1% tryptone and 0.5% yeast extract,
434 supplemented with 1% NaCl) and agar were prepared as previously described[54]. Strains were
435 grown in LB medium with shaking at 220 rpm at either 30˚C, 37˚C, or 42˚C, as indicated.
436 When appropriate, kanamycin (Kan; 25 μg ml^{-1}), chloramphenicol (Cam; 30 μg ml^{-1}) and
437 ampicillin (Amp; 125 μg ml^{-1}) were added.

438

439 **Plasmid construction.** All the plasmids used in this study are listed in Supplementary Table
440 2. Desired genes were amplified from MC4100 chromosomal DNA using the indicated
441 primers (sequences in Supplementary Table 3). Amplified products were digested with
442 indicated restriction enzymes (New England Biolabs), which were also used to digest the
443 carrying vector. After ligation, recombinant plasmids were transformed into competent

444 NovaBlue (Novagen) cells and selected on LB plates containing appropriate antibiotics. DNA
445 sequencing (Axil Scientific, Singapore) was used to verify the sequence of the cloned gene.
446 To generate *tolR*$_{D23R}$ mutant construct, site-directed mutagenesis was conducted using
447 relevant primers listed in Supplementary Table 3 with pET23/42*tolR* as the initial template.
448 Briefly, the entire template was amplified by PCR and the resulting PCR product mixture
449 digested with DpnI for > 1 h at 37˚C. Competent NovaBlue cells were transformed with 1 µl
450 of the digested PCR product and plated onto LB plates containing ampicillin. DNA
451 sequencing (Axil Scientific, Singapore) was used to verify the introduction of the desired
452 mutation.
453
454 **Analysis of [^{32}P]-labelled lipid A.** Mild acid hydrolysis was used to isolate lipid A as
455 previously described[55] with some modifications. 5-ml cultures were grown in LB broth
456 (inoculated from an overnight culture at 1:100 dilution) containing [^{32}P]-disodium phosphate
457 (final 1 µCi ml^{-1}; Perkin Elmer product no. NEX011001MC) till mid-log phase (OD600 ~0.5
458 - 0.7). One MC4100 WT culture labelled with [^{32}P] was treated with EDTA (25 mM pH 8.0)
459 for 10 min prior to harvesting. Cells were harvested at 4,700 x *g* for 10 min, washed twice
460 with 1 ml PBS (137 mM NaCl, 2.7 mM KCl, 10 mM Na_2HPO_4, 1.8 mM KH_2PO_4, pH 7.4)
461 and suspended in PBS (0.32 ml) again. Chloroform (0.4 ml) and methanol (0.8 ml) were
462 added and the mixtures were incubated at room temperature for 20 min with slow shaking (60
463 rpm) to make the one-phase Bligh-Dyer mixture (chloroform:methanol:water = 1:2:0.8).
464 Mixtures were then centrifuged at 21,000 x *g* for 30 min. Pellets obtained were washed once
465 with fresh one-phase Bligh-Dyer system (1 ml) and centrifuged as above. Resulting pellets
466 were suspended in 0.45 ml of sodium acetate (12.5 mM, pH 4.5) containing SDS (1 %) and
467 heated at 100˚C for 30 min. After cooling to room temperature, chloroform and methanol (0.5
468 ml each) were added to create a two-phase Bligh-Dyer mixture (chloroform:methanol:water =

469 2:2:1.8). The lower (organic) phase of each mixture was collected after phase partitioning via
470 centrifugation at 21,000 x *g* for 30 min. This was washed once with upper phase (0.5 ml) of
471 freshly prepared two-phase Bligh-Dyer mixture and centrifuged as above. Finally, all the
472 collected lower phases containing [^{32}P]-labelled lipid A were air-dried overnight. Dried
473 radiolabelled lipid A samples were suspended in 50 µl of chloroform:methanol (2:1) and
474 equal amounts (~1,000 cpm) of radioactivity were spotted on silica-gel coated TLC (Thin
475 Layer Chromatography) plates (Merck). TLCs were developed in chambers pre-equilibrated
476 overnight with solvent system chloroform:pyridine:98 % formic acid:water (50:50:14.6:5).
477 TLC plates were air-dried overnight and later visualized by phosphor imaging (STORM, GE
478 healthcare). The densitometric analysis of the spots obtained on the phosphor images of TLCs
479 was carried out using ImageQuant TL analysis software (version 7.0, GE Healthcare).
480 Average levels of hepta-acylated lipid A (expressed as a percentage of total lipid A in each
481 sample) were obtained from three independent experiments.
482
483 **Sucrose density gradient fractionation.** Sucrose density gradient centrifugation was
484 performed as previously described[56] with some modifications. For each strain, a 10/50-ml
485 culture (inoculated from an overnight culture at 1:100 dilution) was grown in LB broth until
486 OD_{600} reached ~0.5 – 0.7. For radiolabeling, indicated radioisotopes were added from the
487 start of inoculation. Cells were harvested by centrifugation at 4,700 x *g* for 10 min, suspended
488 to wash once in 5 ml of cold Buffer A (Tris-HCl, 10 mM pH 8.0), and centrifuged as above.
489 Cells were resuspended in 6 ml of Buffer B (Tris-HCl, 10 mM pH 8.0 containing 20%
490 sucrose (w/w), 1 mM PMSF and 50 µg ml $^{-1}$ DNase I), and lysed by a single passage through
491 a high pressure French press (French Press G-M, Glen Mills) homogenizer at 8,000 psi.
492 Under these conditions, lipid mixing between inner and outer membranes is minimal[56].
493 Unbroken cells were removed by centrifugation at 4,700 x *g* for 10 min. The cell lysate was

494 collected, and 5.5 ml of cell lysate was layered on top of a two-step sucrose gradient
495 consisting of 40% sucrose solution (5 ml) layered on top of 65% sucrose solution (1.5 ml) at
496 the bottom of the tube. All sucrose (w/w) solutions were prepared in Buffer A. Samples were
497 centrifuged at 39,000 rpm for 16 h in a Beckman SW41 rotor in an ultracentrifuge (Model
498 XL-90, Beckman). 0.8-ml fractions (usually 15 fractions) were manually collected from the
499 top of each tube.
500
501 **Analysis of OMP and LPS levels in isolated OMs.** OM fragments were isolated from 50 ml
502 of cells following growth, cell lysis and application of sucrose density gradient fractionation,
503 as described above. Instead of manual fractionation, OM fragments (~1 ml) were isolated
504 from the 40%/65% sucrose solution interface by puncturing the side of the tube with a
505 syringe. Buffer A (1 ml) was added to the OM fragments to lower the sucrose concentration
506 and reduce viscosity. The OM fragments were then pelleted in a microcentrifuge at 21,000 x
507 *g* for 30 min and then resuspended in 200 - 250 µl Buffer A. Protein concentrations of these
508 OM preparations were determined using Bio-Rad D_C protein assay. The same amount of OM
509 (based on protein content) for each strain was analyzed by reducing SDS-PAGE and
510 immunoblotted using antibodies directed against OmpC, OmpF, LamB, BamA, LptE and
511 LPS.
512
513 **Analysis of steady-state [^{3}H]-glycerol-labelled PL distribution in IMs and OMs.** To
514 specifically label cellular PLs, 10-ml cells were grown at 37˚C in LB broth (inoculated from
515 an overnight culture at 1:100 dilution) containing [2-^{3}H]-glycerol (final 1 µCi ml^{-1}; Perkin
516 Elmer product no. NET022L001MC) until OD_{600} reached ~0.5 - 0.7. Once the desired OD_{600}
517 was achieved, cultures were immediately mixed with ice-cold Buffer A containing CCCP (50
518 µM) to stop the labeling of the cultures. Cells were pelleted, lysed, and fractionated on

519 sucrose density gradients, as described above. 0.8-ml fractions were collected from each tube,
520 as described above, and 300 µl from each fraction was mixed with 2 ml of Ultima Gold
521 scintillation fluid (Perkin Elmer, Singapore). Radioactivity ([^{3}H]-count) was measured on a
522 scintillation counter (MicroBeta$^{2®}$, Perkin-Elmer). Based on [^{3}H]-profiles, IM and OM peaks
523 were identified and peak areas determined after background subtraction (average count of
524 first 5 fractions was taken as background). For each strain, relative [^{3}H]-PL levels in the IM
525 and OM were expressed as a percentage of the sum in both membranes (see Fig. 2a upper
526 panel). The average percent [^{3}H]-PL in the OM for each strain (obtained from three
527 independent experiments) was then compared to that for the WT strain to calculate fold
528 changes (see Fig. 2a lower panel).
529
530 **Determination of PL/LPS ratios in [^{14}C]-acetate labelled OMs (see Extended Data Fig. 5**
531 **for workflow and results).** To specifically label all cellular lipids (including LPS), 10-ml
532 cells were grown at 37˚C in LB broth (inoculated from an overnight culture at 1:100 dilution)
533 containing [1-^{14}C]-acetate (final 0.2 µCi ml^{-1}; Perkin Elmer product no. NEC084A001MC)
534 until OD_{600} reached ~0.5 – 0.7. At this OD, cultures were transferred immediately to ice-cold
535 Buffer A (5 ml), pelleted, lysed, and fractionated on sucrose density gradients, as described
536 above. 0.8-ml fractions were collected from each tube, as described above, and 50 µl from
537 each fraction was mixed with 2 ml of Ultima Gold scintillation fluid (Perkin Elmer,
538 Singapore). Based on [^{14}C]-profiles, IM and OM peaks were identified. OM fractions were
539 then pooled, and treated as outlined below to differentially extract PLs and LPS for relative
540 quantification within each OM pool. For each strain, the whole experiment was conducted
541 and the OM PL/LPS ratio obtained three times.
542 Each OM pool (0.32 ml) was mixed with chloroform (0.4 ml) and methanol (0.8 ml)
543 to make a one-phase Bligh-Dyer mixture (chloroform:methanol:water = 1:2:0.8). The

544 mixtures were vortexed for 2 min and later incubated at room temperature for 20 min with
545 slow shaking at 60 rpm. After centrifugation at 21,000 x *g* for 30 min, the supernatants (S1)
546 were collected. The resulting pellets (P1) were washed once with fresh 0.95 ml one-phase
547 Bligh-Dyer solution and centrifuged as above. The insoluble pellets (P2) were air dried and
548 used for LPS quantification (see below). The supernatants obtained in this step (S2) were
549 combined with S1 to get the combined supernatants (S3), which contained radiolabelled PLs.
550 To these, chloroform (0.65 ml) and methanol (0.65 ml) were added to convert them to two-
551 phase Bligh-Dyer mixtures (chloroform:methanol:water = 2:2:1.8). After a brief vortexing
552 step, the mixtures were centrifuged at 3000 x *g* for 10 min to separate the immiscible phases,
553 and the lower organic phases were collected. These were washed once with equal volumes of
554 water and centrifuged as above, and the lower organic phases (containing radiolabelled PLs)
555 recollected and air dried. Finally, the dried PLs were dissolved in 50 µl of a mixture of
556 chloroform:methanol (2:1). Equal volumes (20 µl) of PL solutions were mixed with 2 ml of
557 Ultima Gold scintillation fluid (Perkin Elmer, Singapore). The [^{14}C]-counts were measured
558 using scintillation counting (MicroBeta$^{2®}$, Perkin-Elmer) and taken as the levels of PLs
559 isolated from the OMs.

560 To quantify LPS, the P2 pellets were suspended in 2X reducing SDS-PAGE loading
561 buffer (40 µl) and boiled for 10 min. Equal volumes (15 µl) were loaded and subjected to
562 SDS-PAGE (15% Tris.HCl). Gels were air-dried between porous films (Invitrogen) and
563 exposed to the same phosphor screen along with standards (GE healthcare). To generate a
564 standard curve for LPS quantification, the WT OM pellet sample was serially diluted two-
565 fold and equal volumes of diluted samples were resolved on SDS-PAGE and dried as above.
566 The densitometric analysis of bands (i.e. LPS from each OM) was carried out using
567 ImageQuant TL analysis software (version 7.0, GE Healthcare). To allow proper comparison

568 and quantification, the LPS gels from triplicate experiments were exposed on the same
569 phosphor screen along with the standards (see Extended Data Fig. 5b)

570 For each strain, the arbitrary PL/LPS ratio in the OM was obtained by taking the
571 levels of PLs (represented by [^{14}C]-counts of PL fraction) divided by the LPS levels
572 (represented by gel band density), averaged across three independent replicates (see Extended
573 Data Fig. 5b, Fig. 2b upper panel). The average PL/LPS ratio in the OM for each strain was
574 then compared to that for the WT strain to calculate fold changes (see Fig. 2b lower panel).

575

576 **Phosphatidylglycerol/Cardiolipin turnover assay (pulse-chase and single time-point (2-**
577 **h) analysis).** PG/CL turnover pulse-chase experiments were performed using the *psd2*
578 background, which accumulated PS and PG/CL during growth at restrictive temperature. For
579 each strain, cells were grown in 70 ml LB broth (inoculated from an overnight culture at
580 1:100 dilution) at the permissive temperature (30˚C) until OD_{600} reached ~0.15 - 0.2. The
581 culture was then shifted for 4 h at the restrictive temperature (42˚C) and labelled with [^{32}P]-
582 disodium phosphate (final 1 μCi ml^{-1}) during the last 30 min at the restrictive temperature
583 (42˚C). After labeling, cells were harvested by centrifugation at 4,700 x *g* for 10 min, washed
584 once with cold LB broth (10 ml) and centrifuged again at 4,700 x *g* for 10 min. Cells were
585 then resuspended in fresh LB broth (70 ml) and the chase was started in the presence of non-
586 radioactive disodium phosphate (1000-fold molar excess) at either the permissive
587 temperature, with or without addition of carbonyl cyanide *m*-chlorophenyl hydrazone (CCCP;
588 50 μM), or at the restrictive temperature in the presence of hydroxylamine (HA; 10 mM). At
589 the start (0 min) and different times (15, 30, 45, 90 and 120 min) during the chase, a portion
590 of the culture (either 15 ml or 10 ml) was collected and mixed immediately with equal
591 volume of ice-cold Buffer A containing CCCP (50 μM) and hydroxylamine (10 mM). Cells
592 were harvested by centrifugation at 4,700 x *g* for 10 min and then resuspended in 6 ml of

593 Buffer B containing CCCP (50 μM) and hydroxylamine (10 mM). Cells were lysed, and
594 fractionated on sucrose density gradients, as described above. 0.8-ml fractions were collected
595 from each tube, as described above. Fractions 7-9 and 12-14 contained the IM and OM
596 fractions, respectively. To extract PLs from the IM and OM pools (2.4 ml), methanol (6 ml)
597 and chloroform (3 ml) were added to make one-phase Bligh-Dyer mixtures. These were
598 incubated at room temperature for 60 min with intermittent vortexing. Chloroform (3 ml) and
599 sterile water (3 ml) were then added to generate two-phase Bligh-Dyer mixtures. After brief
600 vortexing, the lower organic phases were separated from the top aqueous phases by
601 centrifugation at 3,000 x *g* for 10 min. These were washed once with equal volumes of water
602 and centrifuged as above, and the lower organic phases (containing radiolabelled PLs)
603 recollected and air dried. Finally, the dried PLs were dissolved in 40 μl of a mixture of
604 chloroform:methanol (2:1) and spotted onto silica-gel coated TLC plates (Merck). Equal
605 amounts (in cpm) of radioactivity were spotted for each sample. TLCs were developed in pre-
606 equilibrated chambers containing solvent system chloroform:methanol:water (65:25:4). TLC
607 plates were dried, and visualized by phosphor imaging (STORM, GE healthcare).
608 Densitometric analysis of the PL spots on the phosphor image of TLCs was conducted using
609 the ImageQuant TL analysis software (version 7.0, GE Healthcare). The levels of each major
610 PL species were expressed as a percentage of all detected PL species (essentially the whole
611 lane), and plotted against time (see Figs. 3b-e, Extended Data Fig. 7).

612 For single time-point analysis, 30-ml cultures were grown and labelled with [^{32}P]-
613 disodium phosphate (final 1 μCi ml^{-1}) at the restrictive temperature. For strains harboring
614 plasmids used for overexpressing OmpC-Mla components, arabinose (0.2 %) was added
615 during growth at the permissive as well as restrictive temperatures. After washing and
616 resuspension in fresh LB broth (30 ml), the chase was started in the presence of non-
617 radioactive disodium phosphate (1000-fold molar excess) at the permissive temperature. At

618 start (0 h) and 2 h during the chase, a portion of the culture (15 and 10 ml) was collected and
619 processed similarly as pulse chase analysis described above. The levels of PG/CL in the
620 membranes at each time point were expressed as a percentage of the sum of PE, PS and
621 PG/CL. For each strain, IM and OM PG/CL turnover were expressed as the difference
622 between percentage PG/CL levels at 0-h and 2-h time points divided by that at 0-h. Average
623 PG/CL turnover values were obtained from three independent experiments conducted (see
624 Fig. 4, Extended Data Fig. 8).
625
626 **OM permeability assay.** OM sensitivity against SDS/EDTA was judged by colony-forming
627 unit (cfu) analyses on LB agar plates containing indicated concentrations of SDS/EDTA.
628 Briefly, 5-ml cultures were grown (inoculated with overnight cultures at 1:100 dilution) in LB
629 broth at 37˚C until OD_{600} reached ~1.0. Cells were normalized according to OD_{600}, first
630 diluted to OD_{600} = 0.1 (~10^8 cells), and then serial diluted in LB with seven 10-fold dilutions
631 using 96-well microtiter plates (Corning). Two microliters of the diluted cultures were
632 manually spotted onto the plates and incubated overnight at 37˚C.
633
634 **LpxC overexpression (growth curves and viability assay).** For each strain, a 10-ml culture
635 was inoculated in LB broth supplemented with arabinose (0.2 %) from the overnight culture
636 to make the initial OD_{600} of 0.05. Cells were grown at 37˚C and the OD_{600} of the cultures
637 was measured hourly. At the start of growth (0 h) and at 4 and 7 h during growth, 100 µl of
638 cells were collected and then serial diluted in LB/cam with six 10-fold dilutions using 96-well
639 microtiter plates (Corning). Five microliters of the non-diluted and diluted cultures were
640 manually spotted on LB/cam agar plates (no arabinose). Plates were incubated overnight at
641 37˚C.
642

643 **IM (NADH activity) and OM marker (LPS) analysis during sucrose gradient**
644 **fractionation.** The inner membrane enzyme, NADH oxidase, was used as a marker for the
645 IM; its activity was measured as previously described[56]. Briefly, 30 µl of each fraction from
646 the sucrose density gradient was diluted 4-fold with 20 mM Tris.HCl, pH 8.0 in a 96-well
647 format and 120 µl of 100 mM Tris.HCl, pH 8.0 containing 0.64 mM NADH (Sigma) and 0.4
648 mM dithiothreitol (DTT, Sigma) was added. Changes in fluorescence over time due to
649 changes in NADH (λex = 340 nm, λem = 465 nm) concentration was monitored using a plate
650 reader (Perkin Elmer). The activity of NADH oxidase in pooled IM and OM fractions relative
651 to the sum of these fractions was determined.

652 LPS was used as a marker for the OM and detected using LPS dot blots. OM fractions
653 were pooled together and 2 µl of the fractions were spotted on nitrocellulose membranes
654 (Bio-Rad). Spotted membranes were allowed to dry at room temperature for 1 h and then the
655 membranes were probed with antibodies against LPS.

656 .

657 **SDS-PAGE and immunoblotting.** All samples subjected to SDS-PAGE were mixed with
658 2X Laemmli reducing buffer and boiled for 10 min at 100˚C. Equal volumes of the samples
659 were loaded onto the gels. Unless otherwise stated, SDS-PAGE was performed according to
660 Laemmli using the 12% or 15% Tris.HCl gels[57]. Immunoblotting was performed by
661 transferring protein bands from the gels onto polyvinylidene fluoride (PVDF) membranes
662 (Immun-Blot® 0.2 µm, Bio-Rad) using the semi-dry electroblotting system (Trans-Blot®
663 TurboTM Transfer System, Bio-Rad). Membranes were blocked using 1X casein blocking
664 buffer (Sigma). Mouse monoclonal α-OmpC antibody was a gift from Swaine Chen and used
665 at a dilution of 1:5,000[58]. Rabbit α-LptE (from Daniel Kahne)[56] and α-OmpF antisera (Rajeev
666 Misra)[59] were used at 1:5,000 dilutions. Rabbit α-BamA antisera (from Daniel Kahne) was
667 used at 1:40,000 dilution. Mouse monoclonal α-LPS antibody (against LPS-core) was

668 purchased from Hycult biotechnology and used at 1:5,000 dilutions. Rabbit polyclonal α-
669 LamB antibodies was purchased from Bioss (USA) and used at 1:1,000 dilution. α-mouse
670 IgG secondary antibody conjugated to HRP (from sheep) and α-rabbit IgG secondary
671 antibody conjugated to HRP (from donkey) were purchased from GE Healthcare and used at
672 1:5,000 dilutions. Luminata Forte Western HRP Substrate (Merck Milipore) was used to
673 develop the membranes and chemiluminescent signals were visualized by G:BOX Chemi XT
674 4 (Genesys version1.3.4.0, Syngene).
675

676 **References**

677 51. Casadaban, M. J. Transposition and fusion of the *lac* genes to selected promoters
678 in *Escherichia coli* using bacteriophage lambda and Mu. *J. Mol. Biol.* **104**, 541-555
679 (1976)
680 52. Datsenko, K. A. & Wanner, B. L. One-step inactivation of chromosomal genes in
681 *Escherichia coli* K-12 using PCR products. *Proc. Natl. Acad. Sci. U.S.A.* **97**, 6640-
682 6645 (2000)
683 53. Baba, T. *et al.* Construction of *Escherichia coli* K-12 in-frame, single-gene knockout
684 mutants: the Keio collection. *Mol. Syst. Biol.* **2**, 2006.0008 (2006)
685 54. Silhavy, T. J., Berman, M. L. & Enquist, L. W. *Experiments with Gene fusions* (Cold
686 Spring Harbor Laboratory Press, New York, 1984)
687 55. Zhou, Z., Lin, S., Cotter, R. J. & Raetz, C. R. H. Lipid A modifications characteristic
688 of *Salmonella typhimurium* are induced by NH_4VO_3 in *Escherichia coli* K-12. *J. Biol.*
689 *Chem.* **274**, 18503-18514 (1999)
690 56. Chng, S. S., Gronenberg, L. S. & Kahne, D. Proteins required for lipopolysaccharide
691 transport in *Escherichia coli* form a transenvelope complex. *Biochemistry* **49**, 4565-
692 4567 (2010)

693 57. Laemmli, U. K. Cleavage of structural proteins during the assembly of the head of
694 bacteriophage T4. *Nature* **227**, 680-685 (1970)
695 58. Khetrapal, V. *et al.* A set of powerful negative selection systems for unmodified
696 Enterobacteriaceae. *Nucleic Acids Res* **43**, e83 (2015)
697 59. Charlson, E. S., Werner, J. N. & Misra, R. Differential effects of *yfgL* mutation on
698 *Escherichia coli* outer membrane proteins and lipopolysaccharide. *J. Bacteriol.* **188**,
699 7186-7194 (2006)
700 60. Mahalakshmi, S., Sunayana, M. R., SaiSree, L. & Reddy, M. *yciM* is an essential gene
701 required for regulation of lipopolysaccharide synthesis in *Escherichia coli*. *Mol.*
702 *Microbiol.* **91**, 145-157 (2014)
703 61. Ruiz, N., Chng, S. S., Hinikera, A., Kahne, D. & Silhavy, T. J. Nonconsecutive
704 disulphide bond formation in an essential integral outer membrane protein. *Proc. Natl.*
705 *Acad. Sci. U.S.A.* **107**, 12245-12250 (2010)
706 62. Ruiz, N., Falcone, B., Kahne, D. & Silhavy, T. J. Chemical conditionality: a genetic
707 strategy to probe organelle assembly. *Cell* **121**, 307-317 (2005)
708 63. Wu, T. *et al.* Identification of a multicomponent complex required for outer
709 membrane biogenesis in *Escherichia coli*. *Cell* **121**, 235-245 (2005)
710 64. Guzman, L. M., Belin, D., Carson, M. J. & Beckwith, J. Tight regulation, modulation,
711 and high-level expression by vectors containing the arabinose P_{BAD} promoter. *J.*
712 *Bacteriol.* **177**, 4121-4130 (1995)
713 65. Dalebroux, Z. D., Matamouros, S., Whittington, D., Bishop, R. E. & Miller, S. I.
714 PhoPQ regulates acidic glycerophospholipid content of the *Salmonella typhimurium*
715 outer membrane. *Proc. Natl. Acad. Sci. U.S.A.* **111**, 1963-1968 (2014)

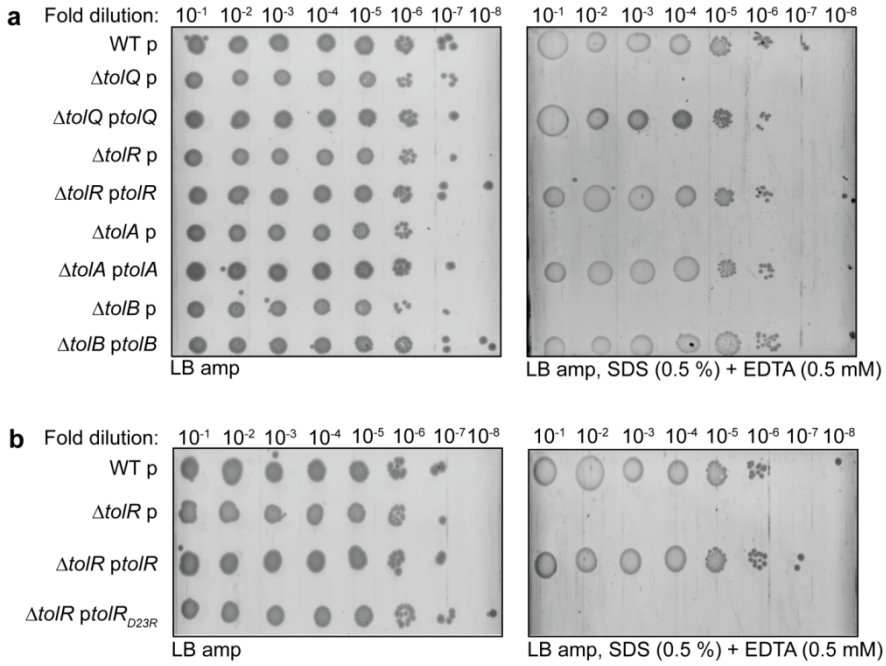

Extended Data Figure 1 | SDS/EDTA sensitivity in *tol-pal* strains can be rescued only by expressing the corresponding functional *tol-pal* gene(s) from the pET23/42 plasmid[23]. Serial dilutions of cultures of wild-type (WT) and indicated *tol-pal* strains harboring pET23/42 empty vector (p), or pET23/42 encoding (**a**) functional or (**b**) non-functional *tol-pal* gene(s) (e.g. p*tolA*), were spotted on LB agar plates containing 125 μg ml^{-1} ampicillin, supplemented with or without SDS (0.5%) and EDTA (0.5 mM) as indicated, and incubated overnight at 37˚C. In the plasmids used, the *tol-pal* gene(s) is placed under the control of the T7 promoter, which is transcribed at low levels by endogenous polymerases. $tolR_{D23R}$ is a non-functional allele encoding TolR protein that is defective in transducing energy derived from the pmf[14].

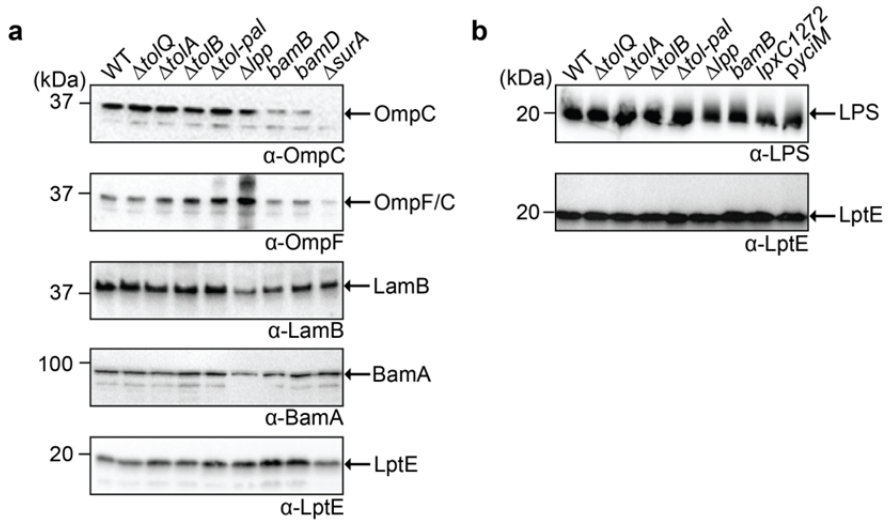

727

728 **Extended Data Figure 2 | *tol-pal* mutations do not affect β-barrel OMP and LPS**
729 **assembly**. Immunoblot analyses of (**a**) indicated OMPs and (**b**) LPS in the OMs of WT and
730 *tol-pal* strains. The OMP assembly mutants (*bamB*, *bamD*, Δ*surA*) and the LpxC-deficient
731 (*lpxC*1272) or YciM-overexpressing (p*yciM*) strains[60] serve as controls for decreased OMP
732 and LPS levels, respectively. The levels of LptE serve as a loading control.

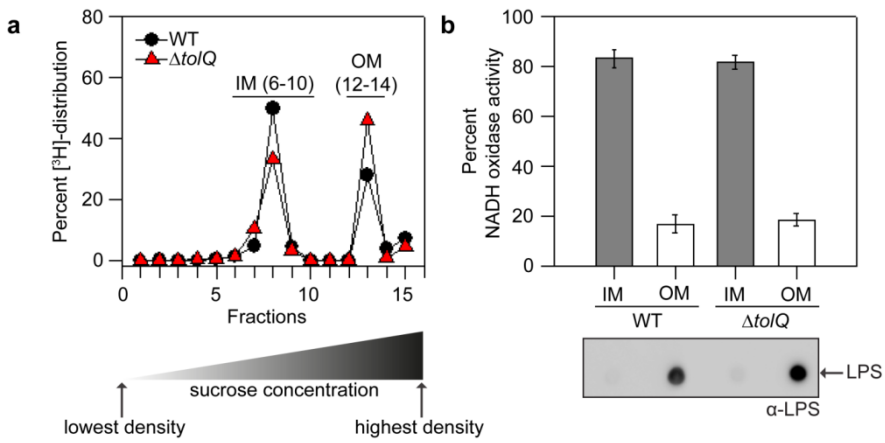

Extended Data Figure 3 | Inner and outer membranes of both WT and *tol-pal* strains are effectively separated via fractionation on sucrose density gradients. a, [^{3}H]-distribution profiles of WT (*black circles*) and Δ*tolQ* mutant (*red triangles*) cell lysates fractionated on a sucrose density gradient. Cells were grown in the presence of [2-^{3}H]-glycerol to specifically label PLs in the IM and OMs. **b**, Percent NADH oxidase activity (*upper panel*) and LPS levels (*lower panel*) (dot blot) in pooled IM and OM fractions from (**a**).

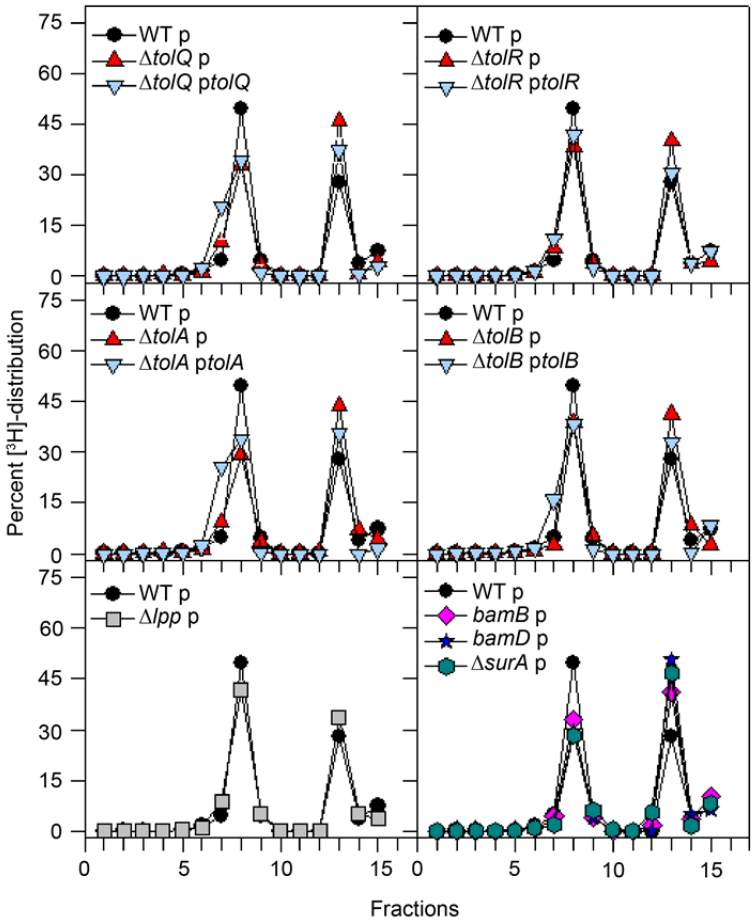

741

742 **Extended Data Figure 4 | Cells lacking the Tol-Pal complex contain more PLs in the**
743 **OM, compared to the IM.** Representative [^{3}H]-distribution profiles of cell lysates from WT
744 (*black circles*), *tol-pal* mutants (*red triangles*), *tol-pal*-complemented strains (*blue inverted*
745 *triangles*), and various control strains, fractionated on sucrose density gradients. Cells were
746 grown in the presence of [2-^{3}H]-glycerol to specifically label PLs in the IMs and OMs. Total
747 [^{3}H]-activities detected in IM (6-10) and OM (12-14) fractions were expressed as a
748 percentage of their sums, averaged across three replicate experiments, and plotted in Fig. 2a.

749

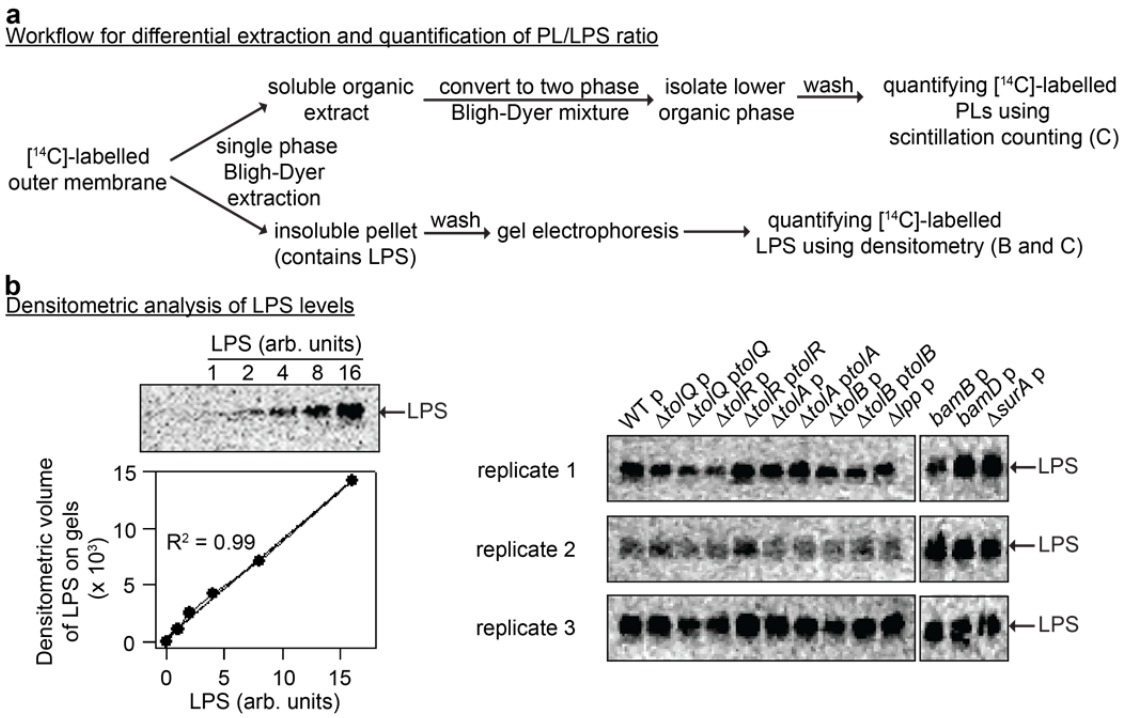

c
Tabulation of [14C]-labelled PLs and LPS levels

Strains	Replicate 1			Replicate 2			Replicate 3			Average	
	PL	LPS	PL/LPS	PL	LPS	PL/LPS	PL	LPS	PL/LPS	PL/LPS	SD
WT p	3640	7.3	497	1517	2.5	597	3602	7.9	457	517	72
Δ*tolQ* p	3715	4.3	860	3014	3.1	975	6471	8.1	797	877	91
Δ*tolQ* p*tolQ*	1970	3.0	663	1321	2.4	548	1990	4.4	457	556	103
Δ*tolR* p	3448	2.6	1306	3452	2.7	1279	6215	5.6	1110	1231	106
Δ*tolR* p*tolR*	6076	9.2	661	2147	4.1	526	6062	10.5	577	588	68
Δ*tolA* p	5342	5.6	961	2971	2.7	1092	5218	7.4	709	921	195
Δ*tolA* p*tolA*	3508	8.6	406	1987	2.9	688	4250	6.2	691	595	163
Δ*tolB* p	3672	4.4	838	2214	2.6	868	3300	4.2	782	830	44
Δ*tolB* p*tolB*	4184	4.2	1006	3014	3.2	957	3890	6.4	610	857	216
Δ*lpp* p	2871	5.0	578	1784	3.0	599	3362	6.4	524	567	38
bamB p	6622	2.8	2340	6806	6.2	1105	6624	7.0	944	1463	764
bamD p	5784	7.7	753	6188	6.3	985	6252	5.5	1143	960	196
Δ*surA* p	7004	5.0	1401	7314	6.8	1076	7528	6.1	1236	1238	163

Extended Data Figure 5 | Cells lacking the Tol-Pal complex accumulate excess PLs (relative to LPS) in the OM. a, Workflow for differential extraction and subsequent quantification of PLs and LPS levels in the [^{14}C]-acetate labelled OMs. **b**, In-gel quantification of [^{14}C]-LPS levels in the OMs of WT, *tol-pal* mutants, *tol-pal*-complemented strains, and various control strains. [^{14}C]-LPS of respective strains separated on SDS-PAGE gels (*right*) were visualized by phosphor imaging and quantified via densitometry using a linear standard curve (*left*). **c**, Tabulation of [^{14}C]-labelled PL levels (scintillation counts), LPS levels (gel densitometry), and arbitrary PL/LPS ratios in the OMs of the indicated

759 strains. The average PL/LPS ratio for each strain was obtained from three independent
760 experiments, and plotted in Fig. 2b.
761

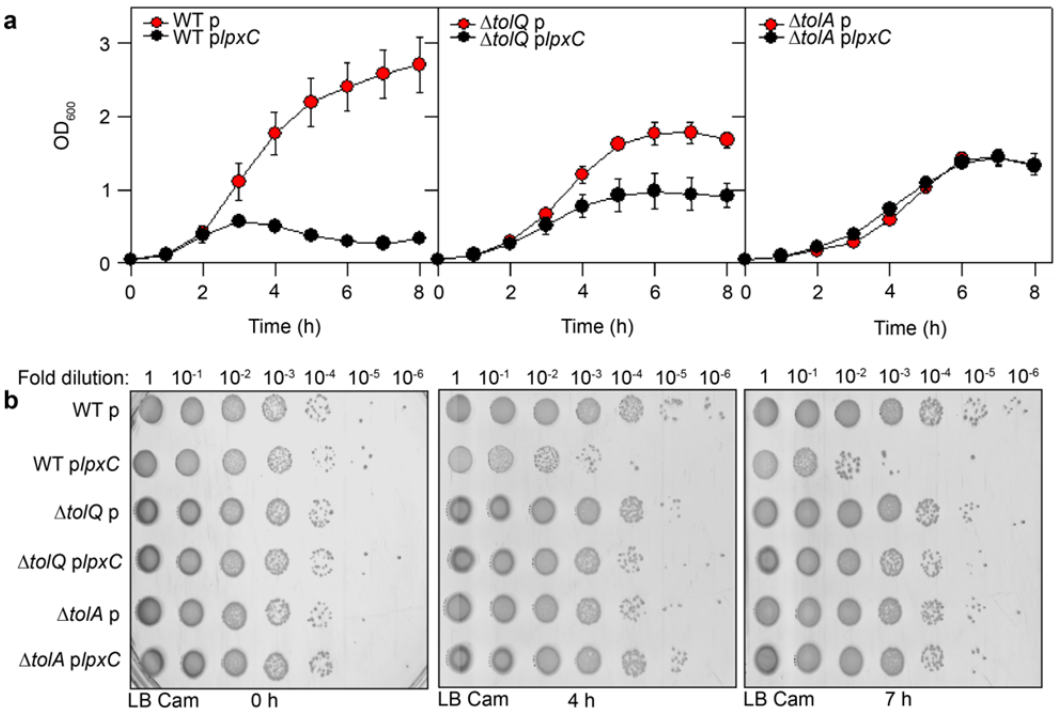

762

763 **Extended Data Figure 6 | *tol-pal* mutants survive toxicity induced by overproduction of**
764 **LpxC, the enzyme catalyzing the first committed step in LPS biosynthesis. a**, Growth
765 profiles of WT, Δ*tolQ* and Δ*tolA* cells harboring either pBAD18cm empty vector (p) or
766 pBAD18cm*lpxC* (p*lpxC*) and grown in the presence of arabinose (0.2%). OD_{600} values were
767 measured every hour during growth. Error bars represent the standard deviation observed
768 from triplicate experiments. **b**, Indicated serial dilutions of 0-, 4- and 7-h cultures of the same
769 strains in (**a**) were spotted on LB agar plates containing 30 μg ml^{-1} cam and incubated
770 overnight at 37˚C.

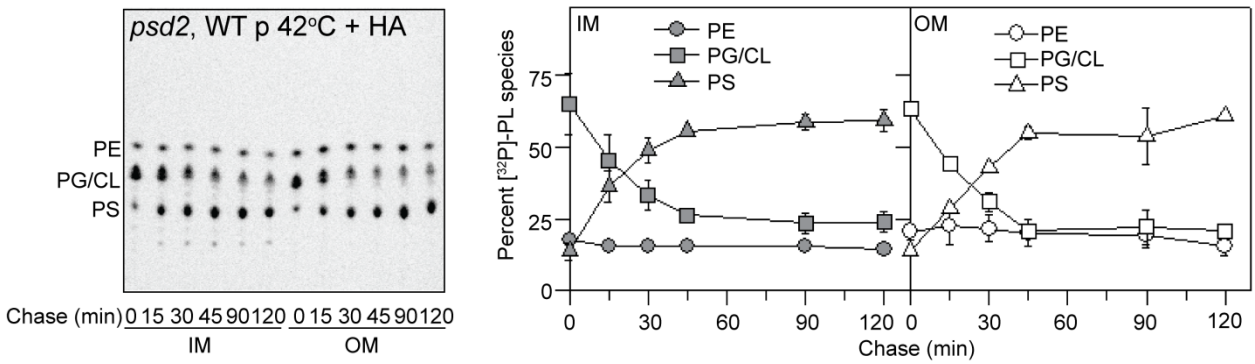

Extended Data Figure 7 | PG/CL is converted to PS in the absence of PSD function. TLC time-course analyses of [^{32}P]-pulse-labelled PLs extracted from the IMs and OMs of the WT strain also harboring the temperature-sensitive *psd2* mutation. Cells were incubated at the restrictive temperature (42˚C, 4 h) and PLs were pulse-labelled with [^{32}P]-phosphate during the last 30 min at the restrictive temperature, and then chased in the presence of excess cold phosphate and hydroxylamine (HA; 10 mM) at the same temperature. HA is a known PSD inhibitor[34]. The percentage levels of PE (circles), PG/CL (squares), and PS (triangles) in the IM (grey symbols) and OM (white symbols) at each time point were quantified and shown on the right. The results clearly showed quantitative PG/CL to PS conversion.

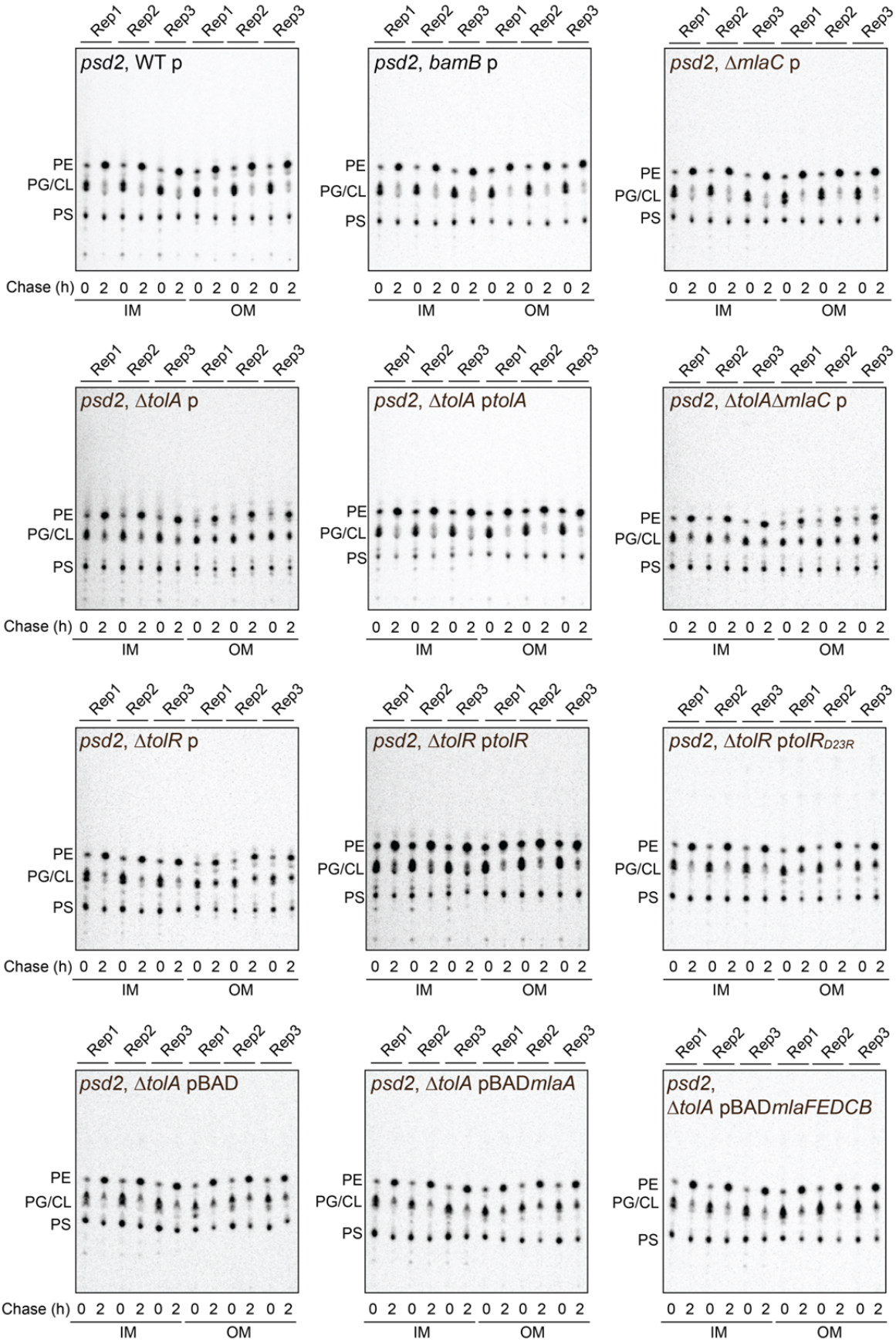
Rep1 Rep2 Rep3 Rep1 Rep2 Rep3
psd2, WT p
psd2, bamB p
psd2, ΔmlaC p
psd2, ΔtolA p
psd2, ΔtolA ptolA
psd2, ΔtolAΔmlaC p
psd2, ΔtolR p
psd2, ΔtolR ptolR
psd2, ΔtolR ptolR$_{D23R}$
psd2, ΔtolA pBAD
psd2, ΔtolA pBADmlaA
psd2, ΔtolA pBADmlaFEDCB
PE
PG/CL
PS
Chase (h) 0 2 0 2 0 2 0 2 0 2 0 2
IM
OM

782

783 **Extended Data Figure 8 | Cells lacking the Tol-Pal complex are defective in OM PG/CL**
784 **turnover.** Single time-point TLC analyses of [^{32}P]-pulse-labelled PLs extracted from the IMs
785 and OMs of indicated strains also harboring the temperature-sensitive *psd2* mutation. Cells
786 were incubated at the restrictive temperature (42˚C, 4 h) and PLs were pulse-labelled with
787 [^{32}P]-phosphate during the last 30 min at the restrictive temperature, and then chased in the
788 presence of excess cold phosphate at the permissive temperature (30˚C) for 2 h. The average
789 extents of PG/CL turnover ([$(\%PG/CL)_{start}$ – $(\%PG/CL)_{2h}$]/[$(\%PG/CL)_{start}$]) in the IM and
790 OM for each strain was obtained from three biological replicate (Reps) experiments, and
791 plotted in Fig. 4.
792

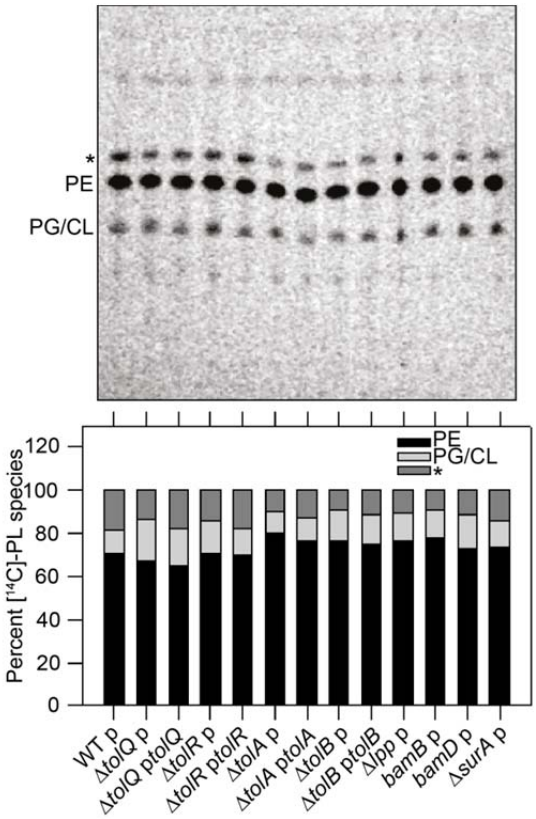

Extended Data Figure 9 | Although cells lacking the Tol-Pal complex accumulate ~50% more PLs in the OM, PL compositions of this membrane are comparable to that in WT cells. TLC analysis of [^{14}C]-labelled PLs extracted from the OMs of WT and indicated mutant strains. Equal amounts of radioactivity were spotted for each sample. An unidentified lipid species that migrated in this solvent system similarly to palmitoylated PG[65] is annotated by an asterisk (*). The percentage levels of PE, PG/CL, and the unidentified lipid were quantified and shown below.

801 **Supplementary Table 1. Bacterial strains used in this study.**

Strains	Relevant genotype	References
MC4100	[*F⁻ araD139* Δ*(argF-lac) U169 rpsL150 relA1 flbB5301 ptsF25 deoC1 ptsF25 thi*]	*51*
BW25113	*F-* Δ*(araD-araB)567* Δ*lacZ4787::rrnB-3 λ- rph-1* Δ*(rhaDrhaB)568 hsdR514*	*53*
NovaBlue	*endA1 hsdR17 (rK12– mK12+) supE44 thi-1 recA1 gyrA96 relA1 lac F' [proA+B+lacIqZ*Δ*M15::Tn10]*	Novagen
NR754	MC4100 *araD*$^{+}$	*24*
MR706	MG1655 *lpxC1272 leuB::Tn10*	*60*
EH150	*psd-2 purA*$^{+}$; temperature-sensitive PSD	*33*
NR1215	NR754 Δ*surA*	*61*
NR698	MC4100 *lptD4213* (*carB*$^{+}$, *Tn10*)	*62*
NR814	MC4100 *bamD::kan*	*63*
NR721	MC4100 *bamB::kan*	*62*
RS101	BW25113 Δ*tolQ::kan*	This study
JW0728	BW25113 Δ*tolR::kan*	*53*
RS102	BW25113 Δ*tolA::kan*	This study
JW5100	BW25113 Δ*tolB::kan*	*53*
RS104	BW25113 Δ*tol-pal::kan*	This study
RS105	BW25113 Δ*lpp::kan*	This study
RS119	MC4100 Δ*tolQ::kan*	This study
RS120	MC4100 Δ*tolR::kan*	This study
RS121	MC4100 Δ*tolA::kan*	This study
RS122	MC4100 Δ*tolB::kan*	This study
RS125	MC4100 Δ*tol-pal::kan*	This study
RS137	MC4100 Δ*lpp::kan*	This study
CZS011	MC4100 Δ*mlaC::kan*	Lab collection
RS173	EH150 Δ*tolR::kan*	This study
RS174	EH150 Δ*tolA::kan*	This study
RS177	EH150 *bamB::kan*	This study
RS178	EH150 Δ*mlaC::kan*	This study
RS180	EH150 Δ*tolA* Δ*mlaC::kan*	This study
JXE082	NR754 Δ*tolQ::kan*	This study
JXE081	NR754 Δ*tolA::kan*	This study

802 **Supplementary Table 2. Plasmids used in this study.**

Plasmids	Description	Plasmid construction		References
		PCR template[a]	PCR primers[b]	
pET23/42	P_{T7} inducible expression vector, contains multiple cloning site of pET42a(+) in pET23a(+) backbone; Amp^R	-	-	*23*
pBAD18cm	P_{BAD} inducible expression vector; Cam^R	-	-	*64*
pBAD33	P_{BAD} inducible expression vector; Cam^R	-	-	*64*
pET23/42*tolQ*	Encodes full length TolQ; Amp^R	Ch. DNA	TolQ-N-NdeI/TolQ-C-AvrII	This study
pET23/42*tolR*	Encodes full length TolR; Amp^R	Ch. DNA	TolR-N-NdeI/TolR-C-AvrII	This study
pET23/42$tolR_{D23R}$	Encodes full length $TolR_{D23R}$; Amp^R	pET23/42*tolR*	TolR-D23R-N/TolR-D23R-C	This study
pET23/42*tolA*	Encodes full length TolA; Amp^R	Ch. DNA	TolA-N-NdeI/TolA-C-AvrII	This study
pET23/42*tolB*	Encodes full length TolB; Amp^R	Ch. DNA	TolB-N-NdeI/TolB-C-AvrII	This study
pET23/42*tol-pal*	Encodes full Tol-Pal complex; Amp^R	Ch. DNA	TolQ-N-NdeI/Pal-C-AvrII	This study
pBAD18cm*lpxC*	Encodes full length LpxC; Cam^R	Ch. DNA	LpxC-N-KpnI/LpxC-C-XbaI	This study
pDSW210-*yciM*	Encodes full length YciM under control of P_{trc}; IPTG-inducible; Amp^R	-	-	*60*
pBAD33*mlaA*	Encodes full length MlaA; Cam^R	Ch. DNA	MlaA-N-KpnI/MlaA-C-XbaI	This study
pBAD33*mlaFEDCB*	Encodes full length MlaFEDCB; Cam^R	Ch. DNA	MlaFEDCB-N-KpnI/MlaFEDCB-C-XbaI	This study

803 [a] Ch. DNA = MC4100 chromosomal DNA.
804 [b] Primer sequences are listed in Table S3.
805

806 **Supplementary Table 3. List of oligonucleotides**

Primer name	Sequence (5'-3')[a]
TolQ-N-NdeI	AGCACATATGACTGACATGAATATCC
TolQ-C-AvrII	ATTCCTAGGTTACCCCTTGTTGCTCTC
TolR-N-NdeI	ACATCATATGGCCAGAGCGCGTGGAC
TolR-C-AvrII	ACACCTAGGTTAGATAGGCTGCGTC
TolA-N-NdeI	ACATCATATGTCAAAGGCAACCGAACAAAAC
TolA-C-AvrII	ACTACCTAGGTTACGGTTTGAAGTCC
TolB-N-NdeI	GCGAATTCATATGAAGCAGGCATTACGAGTA
TolB-C-AvrII	ACTACCTAGGTCACAGATACGGCG
Pal-C-AvrII	ACTACCTAGGTTAGTAAACCAGTACC
LpxC-N-KpnI	ATAAGGTACCTAATTTGGCGAGATAATACGATGATCAAA
LpxC-C-XbaI	ATCGTCTAGATTATGCCAGTACAGCTGAAGG
MlaA-N-KpnI	ATAAGGTACCAAAAAAACAGGGAGACATTTATGAAGCTTC
MlaA-C-XbaI	ATCGTCTAGATTATTCAGAATCAATATCTTTTAAAT
MlaFEDCB-N-KpnI	ATAAGGTACCCGCAAGACGAAGGGTGAATTATGGAGCAGT
MlaFEDCB-C-XbaI	ATCGTCTAGATTAACGAGGCAGAACATCAGCAGG
TolR-D23R-N	ATTGTACCGTTGCTGAGAGTACTGCTGGTGCTG
TolR-D23R-C	CAGCACCAGCAGTACTCTCAGCAACGGTACAAT

807 [a] restriction sites are underlined.